02-2095

UCRL-51902

PHASE DIAGRAMS OF THE ELEMENTS

David A. Young

97

September 11, 1975

Prepared for U.S. Energy Research & Development Administration under contract No. W-7405-Eng-48

Printed in the United States of America
Available from
National Technical Information Service
U. S. Department of Commerce
5285 Port Royal Road
Springfield, Virginia 22151
Price: Printed Copy $___*; Microfiche $2.25

*Pages	NTIS Selling Price
1-50	$4.00
51-150	$5.45
151-325	$7.60
326-500	$10.60
501-1000	$13.60

Distribution Category
UC-4

LAWRENCE LIVERMORE LABORATORY
University of California/Livermore, California/94550

UCRL-51902

PHASE DIAGRAMS OF THE ELEMENTS

David A. Young

MS. date: September 11, 1975

Contents

PHASE DIAGRAMS OF THE ELEMENTS

Abstract

A summary of the pressure-temperature phase diagrams of the elements is presented, with graphs of the experimentally determined solid-solid phase boundaries and melting curves. Comments, including theoretical discussion, are provided for each diagram. The crystal structure of each solid phase is identified and discussed. This work is aimed at encouraging further experimental and theoretical research on phase transitions in the elements.

Introduction

Phase diagrams are useful as compact summaries of large amounts of experimental data. As such they provide an important challenge for theory, since accurate computation of phase transitions typically requires a very high degree of accuracy in solid- and liquid-state theoretical models. To date there have been very few first-principles calculations of one-component pressure-temperature phase diagrams.

The experimental study of phase boundaries has led to the discovery of such unexpected phenomena as isostructural phase transitions and melting curve extrema. A qualitative theoretical understanding of these phenomena has been achieved, and work is continuing in this area. The significance of these phenomena is that they may be quite common at ultrahigh pressures where the atomic shell structure exhibits stepwise breakdown.

Another aspect of phase diagrams that has attracted much attention is the recurrence of patterns in the diagrams of closely related elements. This has been used successfully in predicting the structures and properties of high pressure phases. Thus, certain phase transitions observed at relatively low pressure provide important clues about the behavior of materials at much higher pressure. Deeper theoretical understanding of observed phase behavior will thereby allow quantitative prediction of properties of materials at much higher pressures where experiments are difficult to perform. It may also be

hoped that an adequate theory of phase diagrams for elements will promote the more complex task of describing phase behavior in compounds and multi-component systems.

This report is aimed at encouraging theoretical and experimental research on phase transitions. It is a summary of the experimental data obtained to date on the phase diagrams of the elements. Only solid and liquid phases are shown; the liquid-vapor boundary is not considered here. The temperature abscissa is always referred to zero Kelvin in order to illustrate the true sizes of the various fields of phase stability. Commonly occurring solid phases are labelled with abbreviations: bcc = body-centered cubic (two atoms per unit cell), fcc = face-centered cubic, hcp = hexagonal close packed, and dhcp = double hexagonal. Other solid phases are identified according to the 14 lattice types listed in Appendix A. Dashed lines in the figures indicate extrapolations or poorly determined phase boundaries.

For each element where data are available, a phase diagram is shown and one or more paragraphs of comments are provided. When appropriate, the comments include information on the latest theoretical understanding of the phase diagram. Cursory descriptions of complex crystal structures found among the elements are included in the comments. For details of structures, however, the reader should consult Donohue's The Structures of the Elements.[1]

The bibliography is not exhaustive, since only the most recent papers are cited. However, the reader can easily work back from the references in the recent papers to the earlier ones. The great bulk of the work cited here was done since 1960. Two other useful surveys of phase diagrams for the elements exist,[2,3] but they are already beginning to be dated by continuing research. Very recently, J. F. Cannon has published a critical review of the behavior of the elements at high pressures.[4] Cannon's review and the present one cover much the same ground, and it is hoped that these surveys will fill the gap left by ten years of active research.

Phase Diagrams

HYDROGEN

The phase diagram of hydrogen is shown in Fig. 1. Solid and liquid hydrogen are composed of diatomic molecules interacting according to van der Waals and electric-quadrupole forces. Solid hydrogen and deuterium in thermodynamic equilibrium (i.e., para-H_2 and ortho-D_2) crystallize with the molecules centered on hcp lattice sites. The molecules are essentially freely rotating. For ortho-rich H_2 or para-rich D_2, the stable state at zero Kelvin is cubic, with the molecules centered on an fcc lattice and presumably ordered, with axes pointing along body diagonals.

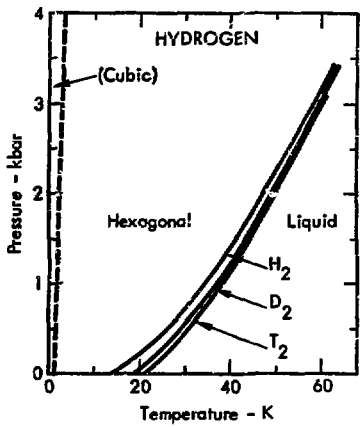

Fig. 1. The phase diagram of hydrogen.

As the cubic lattice is warmed to about 2 K, a first-order transition (probably martensitic,[5] involving the motion of planes of molecules) to the hexagonal phase occurs. Further warming then apparently leads to an order-disorder transition.[6] This occurs as the librating molecules begin to rotate freely. The temperature of the crystallographic transition is a function of pressure and concentration of spin states.

The phase boundary indicated by the dashed line in Fig. 1 is for 70% o-H_2, which has been measured to 5.3 kbar.[7] Theoretical calculations suggest that pure o-D_2 and p-H_2 should have transitions to rotationally ordered cubic lattices at zero Kelvin and compressions corresponding to pressures of a few tens of kilobars.[8] Recently there has been great interest in theoretical and experimental investigations of the insulator-to-metal phase transition in hydrogen, which is exepcted to occur in the megabar range.[9] The three molecular solid isotopes melt in a regular sequence, and the melting curves have been determined to 3.5 kbar.[10]

HELIUM

The phase diagram of helium is shown in Figs. 2-6. The cohesive energy of solid and liquid helium is entirely due to *very* weak van der Waals forces. Because of the strong quantum effects observed in the solid and liquid phases, the phase diagram of helium has been extensively studied and worked out in detail.[11,12] Both isotopes 3 and 4 are liquid at $T = 0$ and $p = 0$ as the result of zero point motion. Under pressure, both liquids solidify. At zero Kelvin and pressures above 0.1 kbar, both solids are hcp and show a transition to fcc around 15 K and above 1 kbar. (Figs. 2 and 5) In ^{3}He, a bcc phase appears below 0.1 kbar and the melting pressure has minimum at 0.32 K (Fig. 3). In ^{4}He, the bcc field is very small, and is replaced by hcp at the lowest temperatures (Fig. 6). The melting curve of ^{4}He has a very flat minimum at 0.78 K. This curve has been extended to 14 kbar, at which pressure the melting temperature is 77 K.

In ^{3}He the normal Fermi liquid persists down to a temperature of 1 mK, where a transition to recently discovered superfluid phases occurs (Fig. 4).[13] The boundary separating the normal Fermi liquid from the A and B superfluid phases represents a second-order phase transition, like

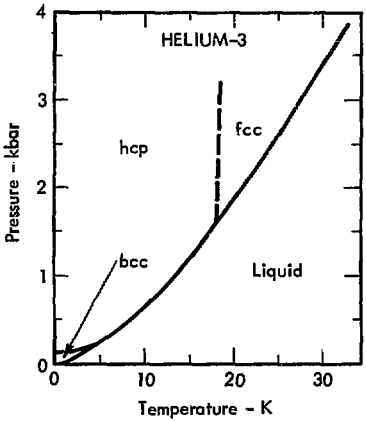

Fig. 2. The phase diagram of helium - 3.

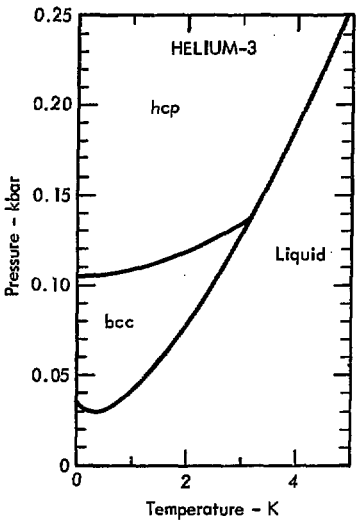

Fig. 3. The phase diagram of helium - 3.

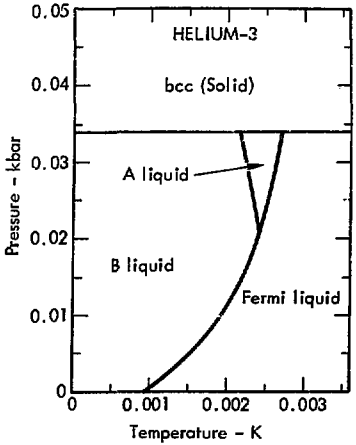

Fig. 4. The phase diagram of helium - 3.

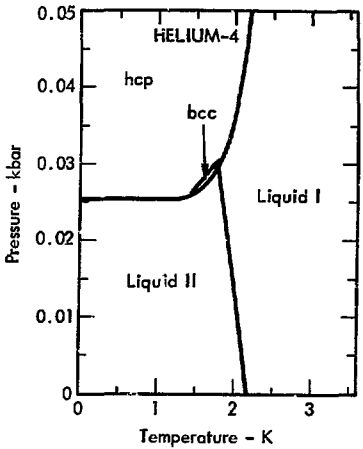

Fig. 6. The phase diagram of helium - 4.

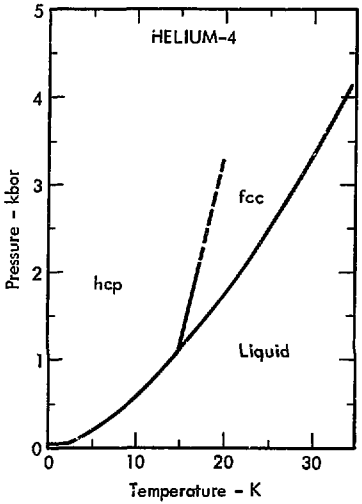

Fig. 5. The phase diagram of helium - 4.

that in ^{4}He. The A-B phase boundary is a first-order phase transition, and it joins the Fermi liquid at a tricritical point. The A and B fluids are thought to be superfluids that result from weak coupling of fermions similar to that found in superconductors. In ^{4}He the normal fluid (I) undergoes a second-order transition (λ-transition) to a superfluid phase (II), which arises from the Bose-Einstein condensation as it is modified by the He-He pair interactions (Fig. 6).

LITHIUM

The phase diagram of lithium is shown in Fig. 7. Upon cooling to

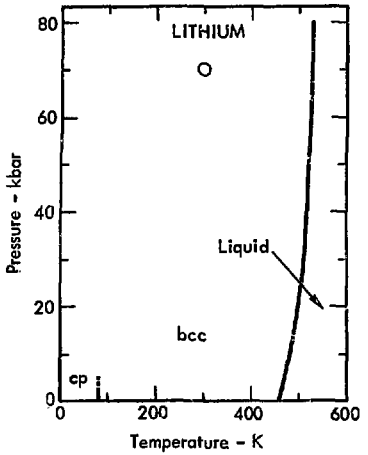

Fig. 7. The phase diagram of lithium.

about 80 K, lithium changes from bcc to a close-packed (cp) structure. The identity of this structure (or structures) is not yet agreed upon. This is a martensitic transition with a considerable temperature hysteresis. The change in transition temperature with pressure is very small, as measurements to 3 kbar have shown.[14] Stager and Drickamer[15] have found a sharp drop in resistance at 70 kbar and 296 K, which is shown by the circle in Fig. 7. The structure of the high pressure phase is not known. The melting curve of lithium has been determined to 80 kbar.[16] The melting temperature becomes nearly constant at this pressure, which suggests that a melting point maximum will occur at a somewhat greater pressure.

BERYLLIUM

The phase diagram of beryllium is shown in Fig. 8. Beryllium has a transition from hcp to bcc just *before* melt. The bcc phase is about 8% more dense, giving rise to the negative slope of the phase boundary. The hcp-bcc phase boundary has been determined to 60 kbar.[17] The same study yielded two other resistance anomalies below 1000 K that appear to correspond to fluctuations in the hexagonal c/a lattice ratio, rather than to genuine phase transitions.

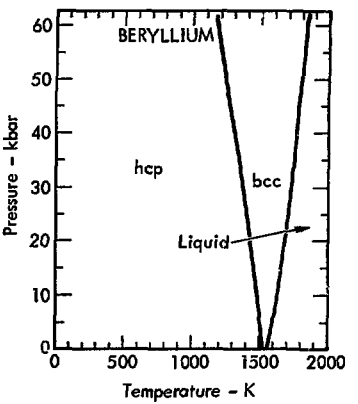

Fig. 8. The phase diagram of beryllium.

Static high pressure resistance measurements by Marder[18] showed a discontinuity at 93 kbar and 293 K, but other investigators have been unable to repeat this result.[19] The melting curve has been determined to 60 kbar.[17]

BORON

Solid boron is covalently bonded. The phase diagram is essentially unknown. Many different crystal structures of boron have been described in the literature,[1] but their relationship to one another is unclear. Furthermore, contamination of boron with metals and the formation of boron-rich borides has a strong effect on the crystal structure. It is suspected that many of the structures reported for pure boron are in fact those of borides.

Solidification of liquid boron yields the "β-rhombohedral" structure with 105 atoms per unit cell and 16 distinct atomic positions. This very complex structure can be resolved into groups of linked icosahedra of boron atoms. It is likely to be the stable phase at low pressures.

Static high pressure resistance measurements up to 250 kbar show no evidence of phase transitions.[20] Wentorf[21] reported a new boron polymorph of unknown structure obtained at pressures above 100 kbar and temperatures near 2000 K, but the probability of sample contamination in this work was large. Boron expands[22] very slightly upon melting near 2350 K,[23] which implies a melting curve with positive slope. The melting curve has not been directly measured.

CARBON

The phase diagram of carbon is shown in Fig. 9. This phase diagram has been the subject of much experimental work owing to the problem of producing artificial diamonds.

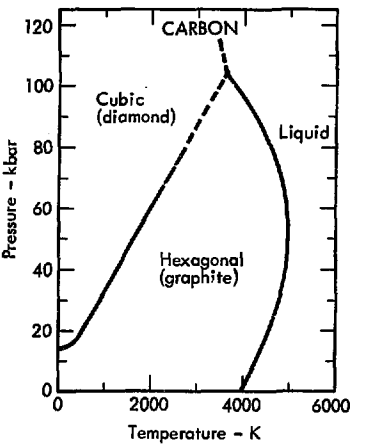

Fig. 9. The phase diagram of carbon.

However, the very high temperatures and pressures involved have made the measurement of the phase boundaries extremely difficult, and the phase diagram cannot be said to be firmly established.

Graphite, the stable phase at low pressures, has hexagonal lattice symmetry. Graphite consists of plane sheets of covalently bonded atoms. The sheets are bonded to each other by weaker van der Waals forces. The high pressure diamond phase is cubic, with eight atoms per unit cell. Each atom is covalently bonded to four neighbors located at the corners of a tetrahedron.

Because diamond is metastable at room temperature and pressure, the free energy difference between graphite and diamond can be computed from measured thermodynamic data, and the graphite-diamond phase boundary can be established.[24] This has been done with reasonable accuracy up to 1200 K and 40 kbar. Beyond this, the actual transformation of graphite to diamond in transition-metal matrices has been carried out.[24] These measurementa extend the phase boundary to 80 kbar. The dashed line is a linear extrapolation of the lower-temperature results. Together with the melting curve, this yields a graphite-diamond-liquid triple point near 100 kbar and 3500 K.

Shock wave experiments[25] up to a few hundred kbar clearly show the graphite-diamond transition, but this is dominated by nonequilibrium effects and the initial state of the graphite. The significance of shock data[26] indicating a new phase at yet higher pressure is still uncertain. Very recently, Vereshchagin's group has obaerved a transition from the diamond to a metallic phase at pressures of approximately 1 Mbar.[27] They also observed that the transition pressure drops with increasing temperature, which is similar to the behavior of the semiconductor-to-metal transitions in silicon and germanium.

The melting temperature of graphite shows a maximum near 5000 K and 50 kbar according to recent work.[28] Uncertainties in the temperature measurements are large. Melting of diamond has not been reported, but the melting curve is assumed to have a negative slope by analogy with silicon.

NITROGEN

The phase diagram of nitrogen is shown in Figs. 10 and 11. Nitrogen in the solid and liquid phases is composed of diatomic molecules weakly bonded to each other by van der Waals and electric-quadrupole forces. Three solid phases are known.[29] In

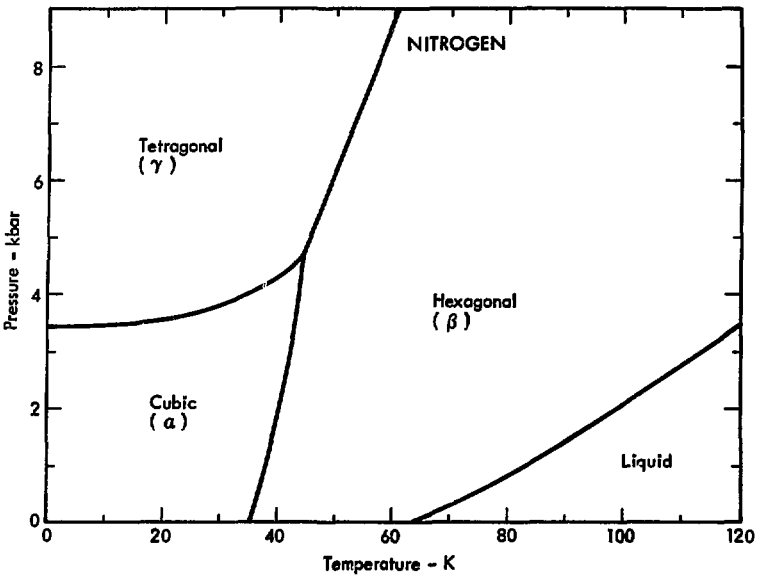

Fig. 10. The phase diagram of nitrogen.

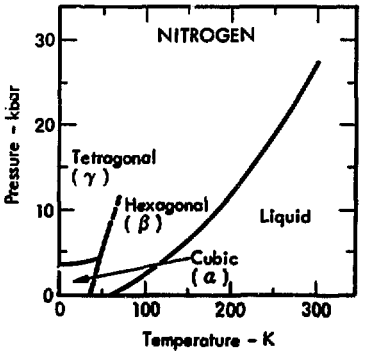

Fig. 11. The phase diagram of nitrogen.

the cubic α phase, the molecules are centered on an fcc lattice with the molecular axes pointing along body diagonals. This ordering is presumably stabilized by quadrupolar forces. At 36 K, the cubic phase transforms to a hexagonal phase in which the molecules are centered on an hcp lattice and are thought to be rotationally disordered. The γ phase is a tetragonal structure with two molecules per unit cell. The molecules are packed in sheets with the molecular axes all aligned and lying in

the plane of the sheet. The direction of the molecular axis shifts by 90° from one sheet to the next. The solid-solid phase boundaries have been determined to about 10 kbar (Fig. 10).[30] The melting curve has been determined to about 25 kbar (Fig. 11).[31]

OXYGEN

The phase diagram of oxygen is shown in Fig. 12. Oxygen in the solid and liquid phases is composed of diatomic molecules weakly bonded by van der Waals and electric-quadrupole forces. Three solid phases are known. The monoclinic α phase is antiferromagnetic, due to the ordering of the spins in the triplet ground state. A transition to the rhombohedral β phase, which is paramagnetic, takes place at 24 K. This transition is definitely first order, although martensitic.[5] Another transition to the cubic γ phase, also paramagnetic, takes place with large volume change at 44 K. This phase shows some rotational disorder. All of these phases may be regarded as close packed with distortions introduced by the non-spherical molecules. The solid-solid phase boundaries have been determined to a few kbar.[32] The melting curve has also been determined to 3.5 kbar.[33]

FLUORINE

The phase diagram of fluorine is shown in Fig. 13. Fluorine in the solid and liquid is composed of diatomic molecules weakly bonded by

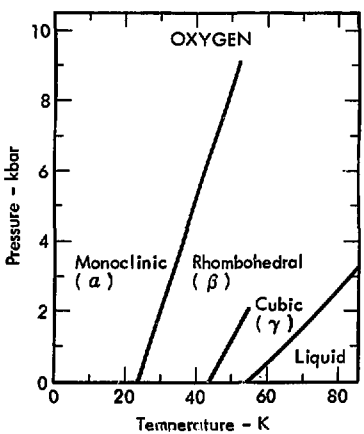

Fig. 12. The phase diagram of oxygen.

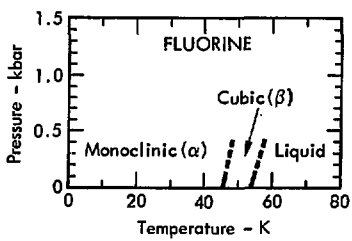

Fig. 13. The phase diagram of fluorine.

van der Waals and electric-quadrupole forces. At low temperatures fluorine is monoclinic with a structure very similar to α-O_2. At 46 K a transition with a large volume change takes place to cubic β-fluorine. This phase is isostructural with γ-O_2, and the lattice is rotationally disordered. The similarity between β-F_2 and γ-O_2 is seen in the close agreement in the transition temperatures and the melt temperatures in the two elements. The α-β phase boundary in Fig. 13 was determined from the ΔH and ΔV of transition.[5,34] The melting curve has been determined to only a few bars.[35]

NEON

The phase diagram of neon is shown in Fig. 14. Neon in the solid and liquid states is composed of atoms weakly bound by van der Waals forces. Solid neon is fcc. The melting curve has been determined to 10 kbar.[36]

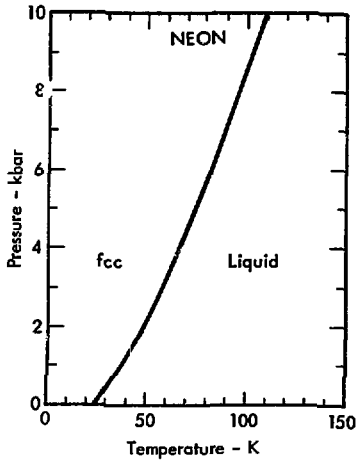

Fig. 14. The phase diagram of neon.

SODIUM

The phase diagram of sodium is shown in Fig. 15. Below 36 K, sodium is hcp. At 36 K a martensitic phase change leads to a bcc structure which persists up to melt. The phase boundary separating the two phases

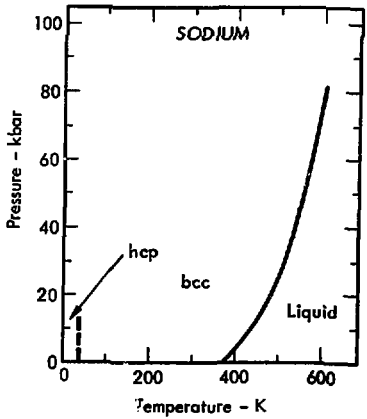

Fig. 15. The phase diagram of sodium.

has not been reported, but the densities are so nearly equal[1] that the initial value of dT/dp should be close to zero, as indicated in Fig. 15. Static high pressure measurements in the solid up to 600 kbar reveal no phase changes.[15] The melting curve has been determined to 80 kbar.[16]

MAGNESIUM

The phase diagram of magnesium is shown in Fig. 16. Solid magnesium is hcp. Resistivity and x-ray measurements on magnesium under static high pressure show indications of a sluggish phase transition near 100 kbar.[37] The structure of the high pressure phase is undetermined. The melting curve has been determined to 40 kbar[38] and the results have been corrected to the atmospheric-pressure melting point in Fig. 16.

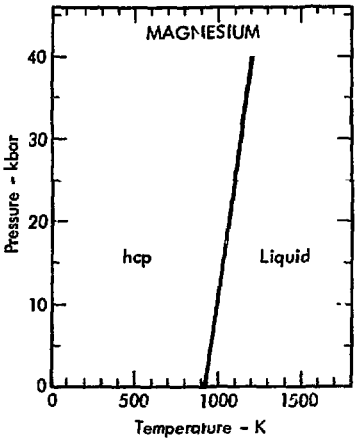

Fig. 16. The phase diagram of magnesium.

ALUMINUM

The phase diagram of aluminum is shown in Fig. 17. Solid aluminum is fcc. Static high pressure measurements tentatively indicate a partial transformation to hcp at 205 kbar.[39] The melting curve has been determined to 60 kbar.[40]

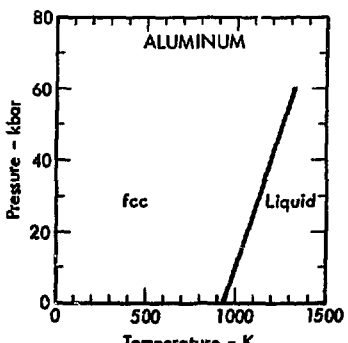

Fig. 17. The phase diagram of aluminum.

SILICON

The phase diagram of silicon is shown in Fig. 18. Normal solid silicon is covalently bonded semiconductor with the cubic diamond structure. Static high pressure measurements show a sharp drop in resistivity near 200 kbar.[41] Subsequent x-ray work showed this phase to have the tetragonal white tin structure.[42] Here each atom has four nearest neighbors and two next nearest neighbors lying slightly farther away. The accurate determination of the phase boundary is complicated by its sensitivity to shear stresses. In addition, recovery of silicon compressed above 100 kbar has yielded a complex cubic form with 16 atoms per unit cell.[43] This uncertainty in the phase diagram is indicated by a dashed line in Fig. 18. At low pressures, solid silicon melts to a more-dense metallic liquid. The melting curve has been measured to 200 kbar, and a clear-cut triple point occurs at 150 kbar.[44] Shock-wave experiments also show phase transitions in the 100-200 kbar region,[45] but their precise nature is unknown.

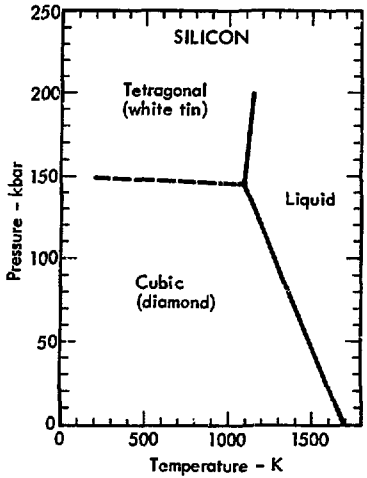

Fig. 18. The phase diagram of silicon.

PHOSPHORUS

The phase diagram of phosphorus is shown in Fig. 19. Of the various allotropic forms of phosphorus that

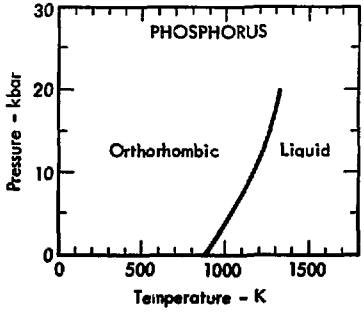

Fig. 19. The phase diagram of phosphorus.

have been prepared, black phosphorus appears to be the most stable phase at atmospheric pressure. Black phosphorus has an orthorhombic structure consisting of puckered layers of covalently bonded atoms.

At room temperature and about 50 kbar, black phosphorus undergoes a phase change to a rhombohedral lattice, isostructural with arsenic.[46] A further transition near 110 kbar to a simple cubic structure was also observed.[46] The rhombohedral lattice is a simple distortion of the simple cubic, and thus the phase transition is easily reversible. Conductivity studies indicate that the cubic phase is metallic.[47] Solid-solid phase boundaries have not been determined. The melting curve of othorhombic black phosphorus has been determined to about 20 kbar.[48,49]

SULFUR

The phase diagram of sulfur is shown in Fig. 20. The literature on the allotropy of sulfur presents the most complex and confused situation of all the elements. Solid sulfur under room conditions is composed of covalently bonded S_8 rings that interact with each other through van der Waals forces. Below 360 K at atmospheric pressure sulfur has an orthorhombic lattice with 128 atoms (16 molecules) per unit cell in a very complex arrangement. Above 360 K, the solid is monoclinic, with 48 atoms (6 molecules) per unit cell. The orientations of two of the six molecules in each unit cell are disordered.

There is much disagreement about the structures of the high pressure phases and the phase boundaries separating them. The phase diagram shown in Fig. 20 is due to Vezzoli, et al.[50-52] The phase boundaries in the solid were detected by means of volumetric, optical, and electrical-resistance techniques.

The phase transitions are often difficult to detect, as indicated by the dashed boundaries in Fig. 19. The large number of phases can be understood as a series of stepwise conformational changes in the S_8 rings with changes in temperature and pressure. The structures of the phases other than the well-known I and II have not been worked out, although there is evidence that phase XII is monoclinic, with closely packed helical chains of atoms similar to the selenium and tellurium structures.[53] Resistance measurements on sulfur compressed to 400 kbar showed no transition to a metallic state.[54]

The melting curve shows a number of definite cusps attributed to the

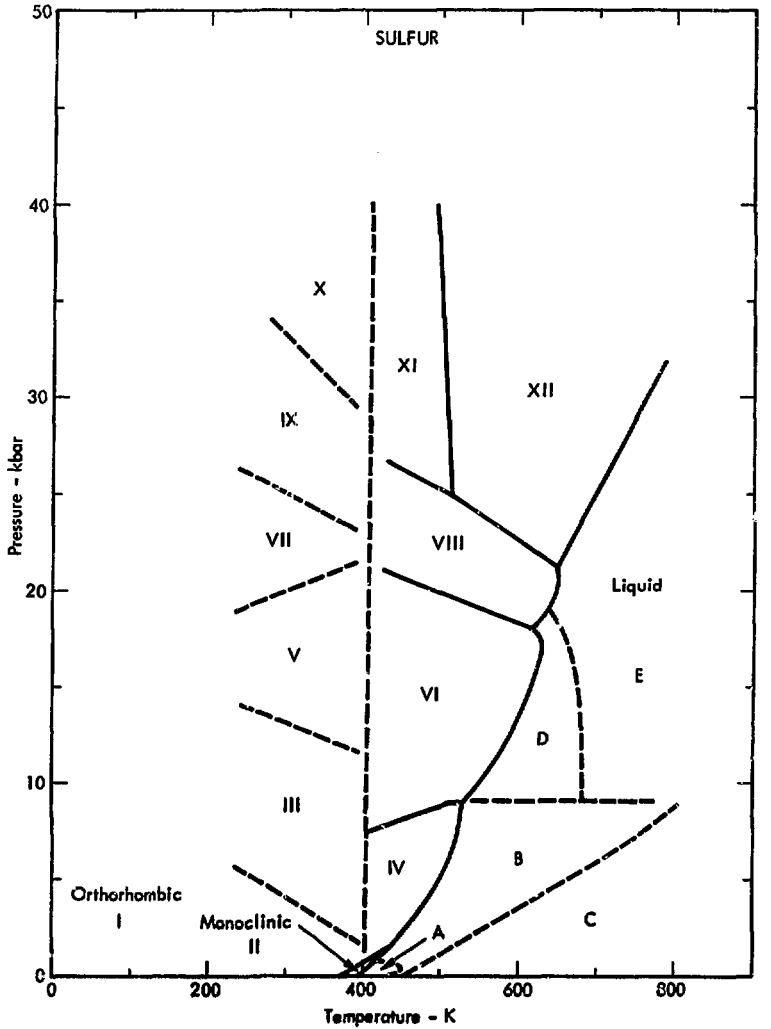

Fig. 20. The phase diagram of sulfur.

intersection of solid-solid phase boundaries. In addition, Vezzoli et al.[52] have discovered a number of "phases" (indicated by letters) in the liquid using DTA techniques. These regions in the liquid appear to be different polymeric states resulting from the breakup of the S_8 rings. The nature of the transitions joining the liquid phases is not clearly understood. The lower portion of the melting curve given by Vezzoli et al. has been independently confirmed.[55]

CHLORINE

The phase diagram of chlorine is shown in Fig. 21. Chrlorine in the solid and liquid states exists as diatomic molecules bonded to neighbors by van der Waals forces. Solid chlorine has an orthorhombic structure, composed of approximately close-packed layers of molecules. The melting curve has been determined to 7 kbar.[56]

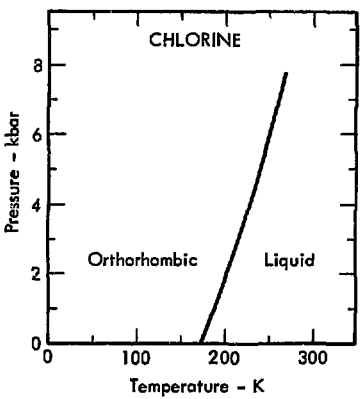

Fig. 21. The phase diagram of chlorine.

ARGON

The phase diagram of argon is shown in Fig. 22. Argon in the solid and liquid is composed of atoms weakly bonded by van der Waals forces. Solid argon is fcc. The melting curve has been determined to 26 kbar.[31]

POTASSIUM

The phase diagram of potassium is shown in Fig. 23. Solid potassium is bcc. No martensitic transition of the

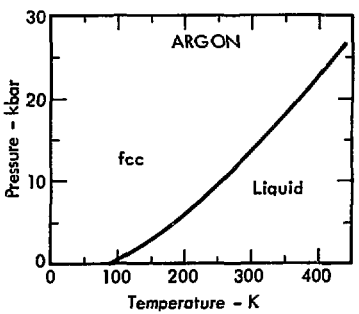

Fig. 22. The phase diagram of argon.

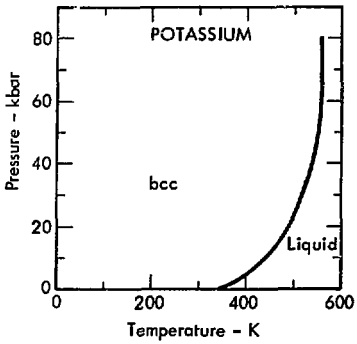

Fig. 23. The phase diagram of potassium.

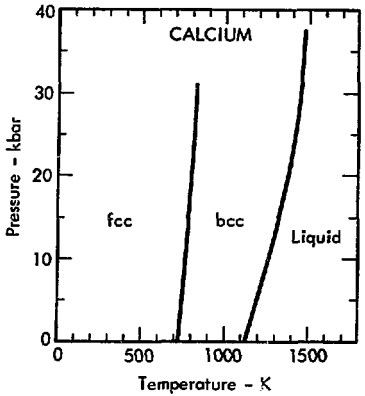

Fig. 24. The phase diagram of calcium.

kind occuring in Li and Na is found in potassium upon cooling to 5 K. However, Stager and Drickamer[15] found two resistance anomalies at 280 kbar and 360 kbar at 77 K. These transitions were not observed at 296 K. The authors suggest that the more dramatic second transition is analogous to the low temperature transition in Li and Na. The melting curve of potassium has been determined to 80 kbar.[16]

CALCIUM

The phase diagram of calcium is shown in Fig. 24. Under room conditions calcium is fcc. Near 700 K at one atmosphere it undergoes a transition to a bcc structure. The phase boundary has been measured to 30 kbar.[57] High pressure resistance measurements at 77 K showed a sharp rise in resistance near 140 kbar and a subsequent sharp drop near 400 kbar.[58] These data were ascribed to two rather sluggish phase transitions, first to a semimetallic, then to a metallic phase. These data are in rough accord with later Soviet work.[59] The melting curve of calcium has been determined to 40 kbar.[57]

SCANDIUM

Scandium is hcp at atmospheric pressure. Static high pressure resistance measurements at room temperature showed no evidence of a phase change to 140 kbar.[60] Shock wave measurements by Carter, et al. showed a kink in the u_s-u_p curve at

approximately 350 kbar.[61] This was ascribed to a sluggish low pressure solid-solid phase change. No kink was found in the shock wave work of Gust and Royce.[62] Scandium melts at 1812 K.[63] The melting curve has not been reported.

TITANIUM

The phase diagram of titanium is shown in Fig. 25. At room temperature and pressure titanium is hcp. A transformation to a bcc phase occurs near 1150 K. The phase boundary has been determined to about 110 kbar, where a triple point occurs.[64,65] The low temperature, high pressure ω phase may be regarded as a distorted bcc lattice with hexagonal symmetry. This structure has three atoms per unit cell and two distinct types of atomic positions.

Shock wave experiments show a strong break in the u_s-u_p curve for titanium, indicating a phase change occurring at 175 kbar.[66] The nature of this phase transition has not been determined. Titanium melts at 1941 K.[63] The melting curve has not been reported.

VANADIUM

Vanadium is bcc. No solid-solid phase transitions have been reported. Vanadium melts at 2178 K.[63] The melting curve has not been reported.

CHROMIUM

The phase diagram of chromium is shown in Fig. 26. Pure chromium is antiferromagnetic below 311 K and paramagnetic above this temperature. Although there has been some controversy about various allotropes of

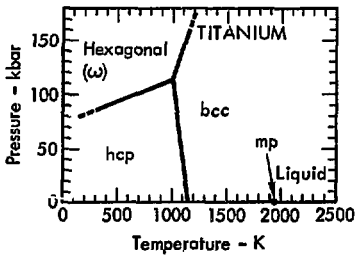

Fig. 25. The phase diagram of titanium.

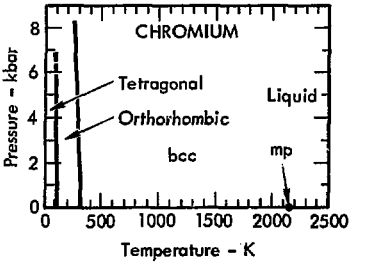

Fig. 26. The phase diagram of chromium.

chromium, it is probable that the paramagnetic phase is simple bcc up to the melting point. Below 311 K, the paramagnetic phase transforms to an antiferromagnetic phase by a first-order phase transition. This phase is in a spin-density wave state in which the polarization is perpendicular to the wave vector.[67] This magnetic state is inconsistent with the retention of full cubic symmetry, and the lattice instead takes on a very slight orthorhombic distortion of the bcc lattice.

At 123 K, another first-order tr sition occurs to a new antiferromagnetic spin-density wave state in which the polarization and wave vectors are parallel. This phase has a small tetragonal distortion of the bcc lattice. The lattice distortions in the magnetic phase are too small to be detected with present x-ray techniques. The phase boundaries have been determined to 8 kbar.[68,69] Static pressure measurements at room temperature to 55 kbar show no other phase changes.[70] Chromium melts at 2148 K.[63] The melting curve has not been reported.

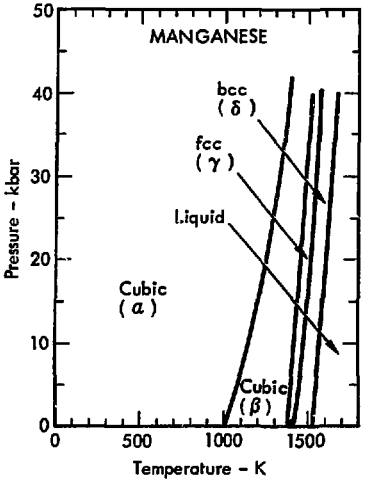

Fig. 27. The phase diagram of manganese.

MANGANESE

The phase diagram of manganese is shown in Fig. 27. There are four allotropes, all of cubic symmetry. The α form has a complex body centered cubic lattice with 58 atoms per unit cell and 4 different types of atomic positions. At atmospheric pressure near 1000 K, a transition occurs to the β form, thought to have 20 atoms per unit cell and 2 types of atomic positions. Near 1370 K a transition to the fcc γ phase occurs, and near 1520 K a further transition to the bcc δ phase occurs. The phase boundaries and the melting curve have been determined to 40 kbar.[71]

IRON

The phase diagram of iron is shown in Fig. 28. The phase diagram and especially the melting curve of iron is of great interest because of the problem of the state of the earth's core and the origin of the geomagnetic field. Under room conditions iron is ferromagnetic and has a bcc structure. At 1044 K it passes through the Curie point and near 1200 K it transforms to the fcc phase. The bcc phase once again becomes stable before melting. Above 100 kbar, the bcc phase transforms to a nonferromagnetic hcp phase. The α-γ, α-ε, and γ-ε phase boundaries have been determined to 200 kbar.[72] The γ-δ transition and the melting curve have been determined to 52 kbar, where they meet in a triple point.[73] The melting curve of the γ phase has been extended about 5 kbar beyond the triple point.[73]

COBALT

The phase diagram of cobalt is shown in Fig. 29. At room temperature cobalt is hcp. At a temperature depending on the sample grain size, a sluggish phase change to fcc occurs. For large crystal grains the transformation temperature is 661 K. The phase boundary has been measured to 50 kbar.[38] Cobalt melts at 1765 K.[63] The melting curve has not been reported.

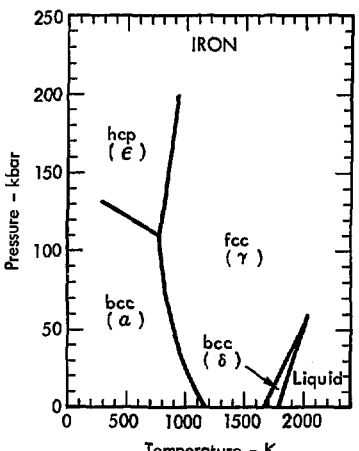

Fig. 28. The phase diagram of iron.

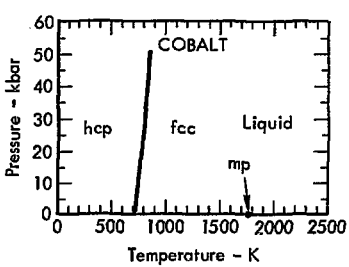

Fig. 29. The phase diagram of cobalt.

NICKEL

The phase diagram of nickel is shown in Fig. 30. Solid nickel is fcc. The melting curve has been determined to 80 kbar.[38,74]

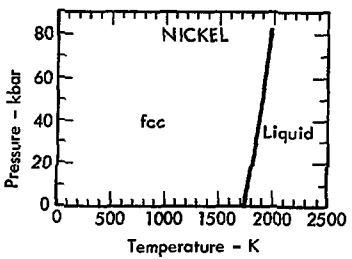

Fig. 30. The phase diagram of nickel.

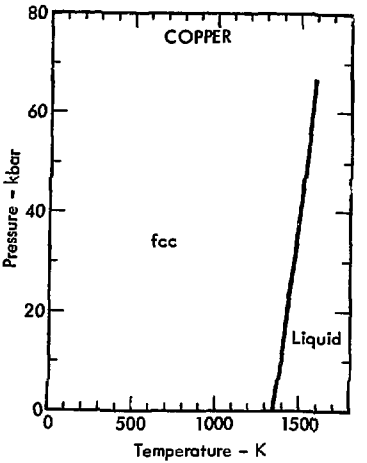

Fig. 31. The phase diagram of copper.

COPPER

The phase diagram of copper is shown in Fig. 31. Solid copper is fcc. The melting curve has been determined to 65 kbar.[75]

ZINC

The phase diagram of zinc is shown in Fig. 32. Solid zinc has a distorted hcp lattice, with the c/a ratio considerably greater than ideal. Under pressure, this ratio shows unusual fluctuations, but no clear-cut solid-solid phase changes are found up to 200 kbar.[76] The melting curve has been determined to 60 kbar.[77]

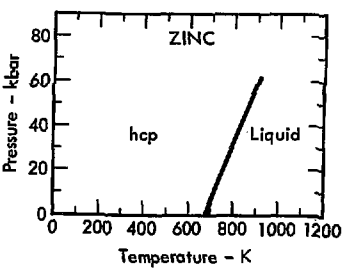

Fig. 32. The phase diagram of zinc.

GALLIUM

The phase diagram of gallium is shown in Fig. 33. Solid gallium at atmospheric pressure has an orthorhombic structure with eight atoms per unit cell. Each atom in this structure has one nearest neighbor and six other near neighbors somewhat farther away. At atmospheric pressure gallium melts just above room temperature, and the melting temperature initially decreases with increasing pressure. Gallium II is probably body centered tetragonal. The high-temperature gallium-III phase is a complex orthorhombic lattice with 40 atoms per unit cell. The phase boundaries, including the melting curve, have been determined to 75 kbar.[78,79]

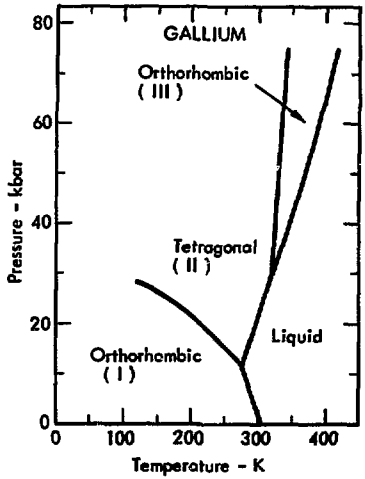

Fig. 33. The phase diagram of gallium.

GERMANIUM

The phase diagram of germanium is shown in Fig. 34. Solid germanium under room conditions is a semiconductor with the cubic diamond structure. Above 100 kbar shock wave[80] and electrical resistance measurements[41] indicate the appearance of a new phase. This phase is metallic, with the tetragonal white tin structure. There remains some uncertainty concerning new phases obtained from quenching experiments.[81] The cubic-tetragonal phase boundary and the

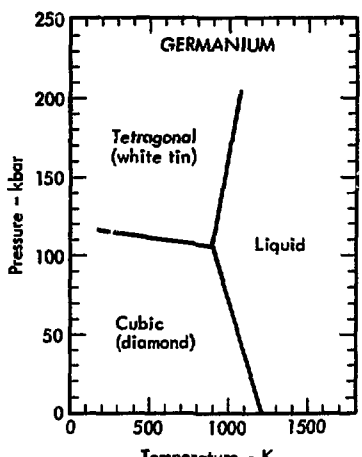

Fig. 34. The phase diagram of germanium.

melting curve have been determined up to 200 kbar.[44]

ARSENIC

The phase diagram of arsenic is shown in Fig. 35. At atmospheric pressure arsenic crystallizes in the primitive rhombohedral lattice characteristic of the group VB elements. High pressure resistance measurements showed no anomaly up to 200 kbar.[82] However, arsenic that had been compressed to 150 kbar showed a tetragonal structure, which may represent a high pressure phase.[83] The melting curve has been determined up to 60 kbar.[84]

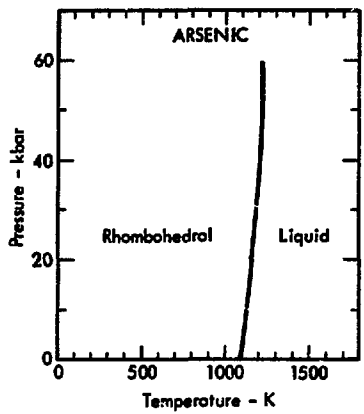

Fig. 35. The phase diagram of arsenic.

SELENIUM

The phase diagram of selenium is shown in Fig. 36. Solid selenium at low pressure has a hexagonal crystal structure composed of covalently bonded helical chains of atoms. In this state selenium is a semiconductor. Near 130 kbar, a resistance discontinuity is observed, and selenium becomes a metallic conductor.[85,86] An attempt to determine the structure of this high pressure form was unsuccessful.[87] The melting curve has been determined to 60 kbar.[88-90] It shows a clear maximum in temperature.

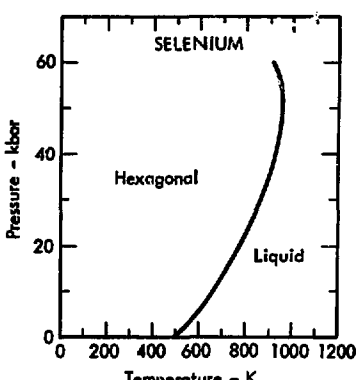

Fig. 36. The phase diagram of selenium.

BROMINE

The phase diagram of bromine is shown in Fig. 37. Solid bromine is composed of diatomic molecules held together by weak van der Waals forces. The solid has an orthorhombic structure, analogous to chlorine. Indirect evidence for a phase transition in solid bromine at 35 kbar has been reported,[91] but no details of the phase boundary or the structure of the new phase are available. The melting curve has been determined to 10 kbar.[56,89]

KRYPTON

The phase diagram of krypton is shown in Fig. 38. Solid and liquid krypton consist of atoms bonded by weak van der Waals forces. The solid is fcc. The melting curve has been determined to 12 kbar.[36,92]

RUBIDIUM

The phase diagram of rubidium is shown in Fig. 39. At low pressures solid rubidium is bcc. Bundy and Strong found a sharp resistance jump near 75 kbar and room temperature.[93] Stager and Drickamer found a sharp rise in resistance near 200 kbar at two temperatures.[15] Soviet work confirmed the 75 kbar transition, but found the next transition near 135-140 kbar rather than 200 kbar.[59] The lower transition is indicated in Fig. 39 by a dashed line. These transitions are thought to correspond to those observed in cesium at low pressure. The upper transition is likely to be due to a shift in the electronic configuration of the rubidium atoms. The melting curve has been determined to 80 kbar.[16] The melting temperature appears to be approaching a maximum near 80 kbar.

STRONTIUM

The phase diagram of strontium is shown in Fig. 40. Under room conditions strontium is metallic with an fcc structure. With increasing pressure at room temperature or below, strontium becomes semimetallic.[94] Near 35 kbar, a phase transition to the metallic bcc structure occurs. The unusual change from a more efficient to a less efficient packing with increasing pressure appears to be due largely to the electronic transitions mentioned. Beyond the 35 kbar transition, strontium shows metallic conductivity with no indication of further transitions up to 500 kbar.[58] The fcc-bcc phase boundary intersects the p = 0 axis at 830 K. This boundary and the melting curve have been determined to 40 kbar.[57]

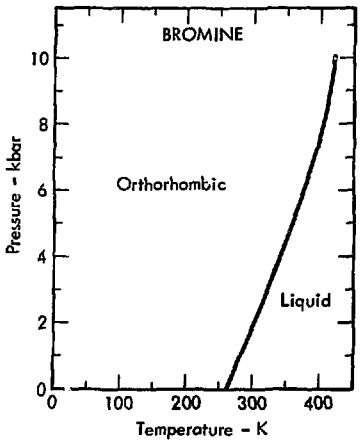

Fig. 37. The phase diagram of bromine.

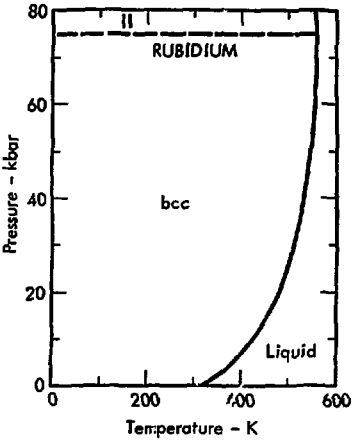

Fig. 39. The phase diagram of rubidium.

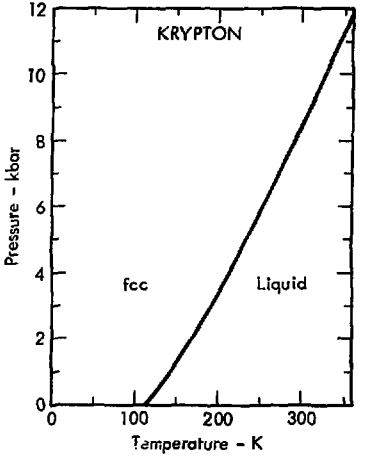

Fig. 38. The phase diagram of krypton.

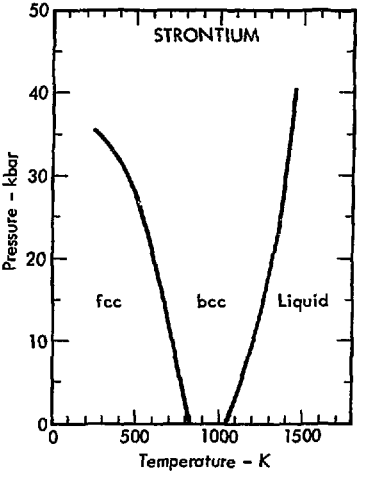

Fig. 40. The phase diagram of strontium.

YTTRIUM

Solid yttrium at low pressure is hcp. Above 110 kbar, yttrium becomes a superconductor.[95] A study of the pressure dependence of the transition temperature indicates the presence of several superconducting modifications.[96] However, these modifications are not thought to have different crystal structures, but rather arise from slight changes in band structure.

Static resistance measurements to 250 kbar show no phase transition anomalies.[97] Shock-wave experiments by Gust and Royce showed a kink in the the u_s-u_p curve at 280 kbar.[62] The authors suggested that the kink indicated the stiffening of the solid as inner electron cores overlapped. Carter, *et al. saw a kink in the* u_s-u_p curve at 370 kbar and suggested a sluggish low pressure transition as an explanation.[61] Yttrium melts at 1775 K.[63] The melting curve has not been reported.

ZIRCONIUM

The phase diagram of zirconium is shown in Fig. 41. Zirconium under room conditions is hcp. Under compression it transforms to the hexagonal ω phase isostructural with ω-titanium. This is a distorted bcc phase. Near 1140 K at atmospheric pressure the hcp phase transforms to bcc. The triple point joining the three phases occurs near 60 kbar and 1000 K. The phase boundaries have been worked out to 70 kbar.[65] Vereshchagin observed a sharp change of slope in the resistance as a function of pressure near 100 kbar, but what this means is unclear.[97] A shock-wave study of zirconium showed a sharp break in the u_s-u_p curve at 260 kbar, which presumably indicates a phase change.[66] Zirconium melts at 2123 K.[63] The melting curve has not been reported.

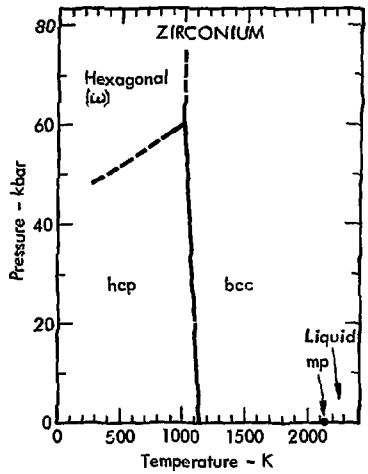

Fig. 41. The phase diagram of zirconium.

NIOBIUM

Solid niobium is bcc. No resistance anomalies have been found below 250 kbar.[97] Niobium melts at 2741 K.[63] The melting curve has not been reported.

MOLYBDENUM

The phase diagram of molybdenum is shown in Fig. 42. Solid molybdenum is bcc. An approximate melting curve has been determined to 90 kbar.[98]

TECHNETIUM

Solid technetium is hcp. Technetium melts at 2443 K.[63] The melting curve has not been reported.

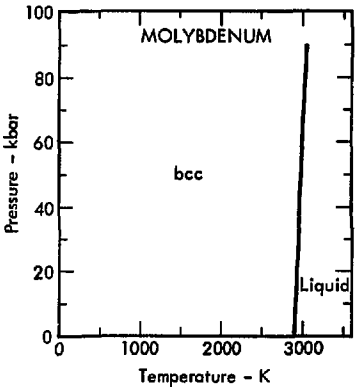

Fig. 42. The phase diagram of molybdenum.

RUTHENIUM

Solid ruthenium is hcp. Compression to 400 kbar at room temperature showed no change of phase.[99] Ruthenium melts at 2553 K.[63] The melting curve has not been reported.

RHODIUM

The phase diagram of rhodium is shown in Fig. 43. Solid rhodium is fcc. The melting curve has been approximately determined to 80 kbar.[38,74]

PALLADIUM

Solid palladium is fcc. Palladium melts at 1825 K.[63] The melting curve has not been reported.

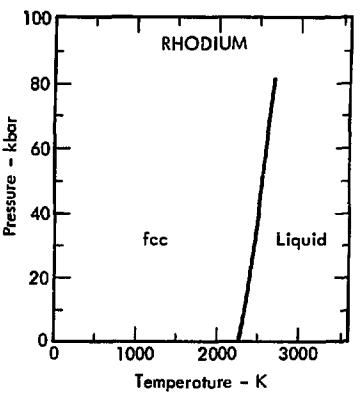

Fig. 43. The phase diagram of rhodium.

SILVER

The phase diagram of silver is shown in Fig. 44. Solid silver is fcc. Compression to 300 kbar at room temperature shows no evidence of a phase change.[100] The melting curve has been determined to 65 kbar.[75]

CADMIUM

The phase diagram of cadmium is shown in Fig. 45. Solid cadmium is hcp. Compression in the 100-200 kbar range shows small anomalies in the resistance and hexagonal c/a ratio, and a sluggish phase transition has been suggested as an explanation.[37] Independent resistance measurements to 250 kbar showed no strong anomalies.[97] The melting curve has been determined to 50 kbar.[38]

INDIUM

The phase diagram of indium is shown in Fig. 46. Solid indium is body centered tetragonal. Compression at room temperature to 300 k ar shows no indication of any phase changes.[101] The melting curve has been determined to 80 kbar.[78]

TIN

The phase diagram of tin is shown in Fig. 47. Below 290 K at

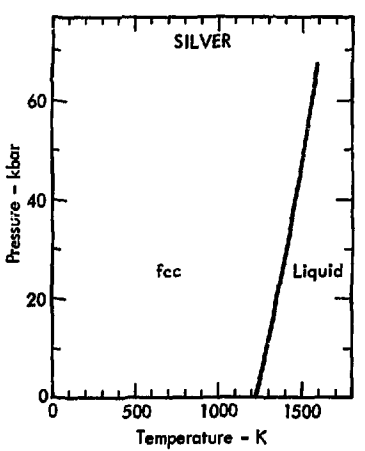

Fig. 44. The phase diagram of silver.

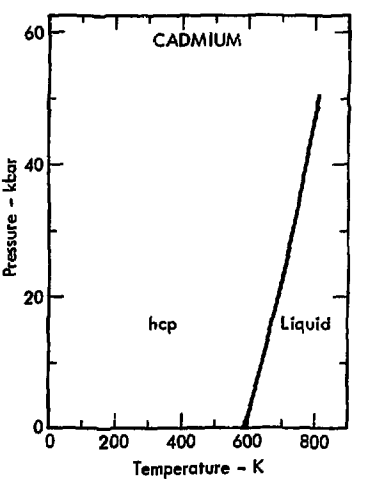

Fig. 45. The phase diagram of cadmium.

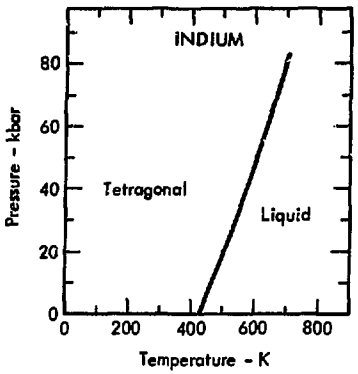

Fig. 46. The phase diagram of indium.

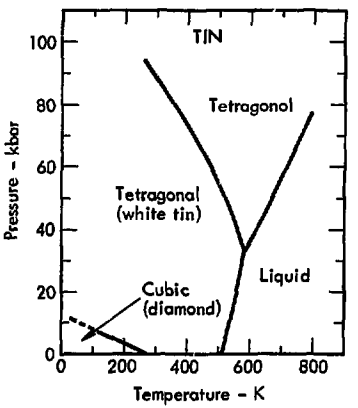

Fig. 47. The phase diagram of tin.

atmospheric pressure, tin is cubic diamond like silicon and germanium. Above this temperature tin has the tetragonal white tin structure with four atoms per unit cell. In this structure each tin atom has four nearest neighbors at the vertices of a flattened tetrahedron. Two more neighbors lie slightly farther away.

The diamond-to-white-tin boundary has been determined to about 50 K and 10 kbar.[102] At room temperature near 90 kbar, the white tin transforms to a body-centered tetragonal structure with two atoms per unit cell. The boundary joining the two phases has been approximately determined to 95 kbar.[103,104] The melting curve has also been determined to 75 kbar.[103,104]

ANTIMONY

The phase diagram of antimony is shown in Fig. 48. Solid antimony under room conditions is rhombohedral, isostructural with arsenic. At room temperature, antimony has two phase transitions, one near 70 kbar and one near 85 kbar (circles).[105] The 70-kbar transition is sluggish and apparently has a very small volume change. The phase II structure is simple cubic, which corresponds to the elimination of the low pressure

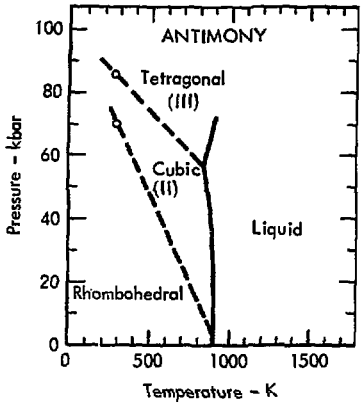

Fig. 48. The phase diagram of antimony.

rhombohedral distortion. The transition at 85 kbar is more strongly marked, with noticeable volume and resistance changes.[106] The structure of phase III is uncertain, but recent work suggests a tetragonal structure analogous to that found in arsenic at high pressures.[83] Phase III shows good metallic conductivity.[82] The melting curve has been determined to 70 kbar.[34,107] Two cusps, indicating triple points, have been found, one at 3.9 kbar, and the other at 57 kbar. Stishov and Tikhomirova[107] assumed that the two triple points corresponded to the two room temperature transitions, as indicated in Fig. 48.

TELLURIUM

The phase diagram of tellurium is shown in Fig. 49. Solid tellurium under room conditions is a semiconductor, with a hexagonal structure composed of covalently bonded helices packed together. This structure can be regarded as a distortion of the simple cubic lattice. Near 40 kbar at room temperature (circle), a transition to a metallic phase occurs. The structure of this phase has not yet been determined.[108] Near 70 kbar at room temperature (circle), a further transition to a rhombohedral lattice occurs.[108] This phase is isostructural with β-polonium. Studies of superconductivity at high pressures indicate possible new

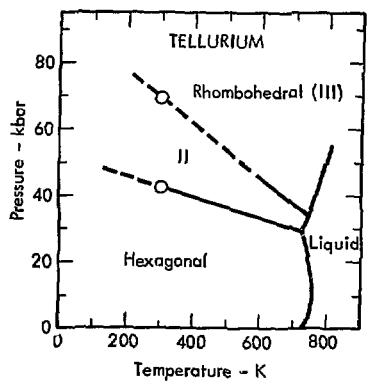

Fig. 49. The phase diagram of tellurium.

phases at still higher pressures.[109] The solid-solid phase boundaries and the melting curve have been determined to about 70 kbar.[110] A definite maximum in the melting temperature is found near 10 kbar.

IODINE

The phase diagram of iodine is shown in Fig. 50. Solid iodine at low pressures is composed of diatomic molecules in an orthorhombic lattice, isostructural with solid bromine and chlorine. No clearly defined phase transition has been found at moderate pressures,[111] but an x-ray study of the solid to 60 kbar showed a continuous shifting of x-ray reflections.[112] This was interpreted as a shifting of the orientations of the diatomic molecules within the orthorhombic unit cell.

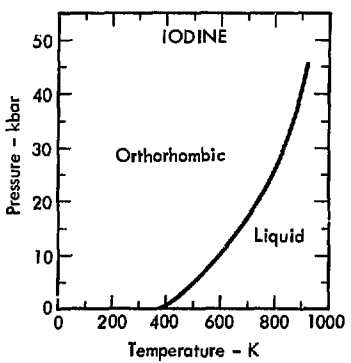

Fig. 50. The phase diagram of iodine.

At higher pressures, above 100 kbar, the resistance of iodine drops rapidly to a metallic value.[113] Here it is thought that the I_2 molecules dissociate into an atomic metallic structure. It is not clear whether this is a continuous or an abrupt transition. Shock wave experiments on iodine show a strong break in the plot of u_s vs u_p at approximately 700 kbar.[114] Given a transition to the metallic phase at a much lower pressure, this break is likely to represent a phase transition from one metallic phase of iodine to another. The melting curve has been determined to 50 kbar.[89,115]

XENON

The phase diagram of xenon is shown in Fig. 51. Solid and liquid xenon are composed of atoms bonded by weak van der Waals forces. Solid xenon is fcc. The melting curve has been determined to 7 kbar.[92]

CESIUM

The phase diagram of cesium is shown in Fig. 52. Cesium has been intensively studied because of its unusual properties. Solid cesium at atmospheric pressure is bcc. At

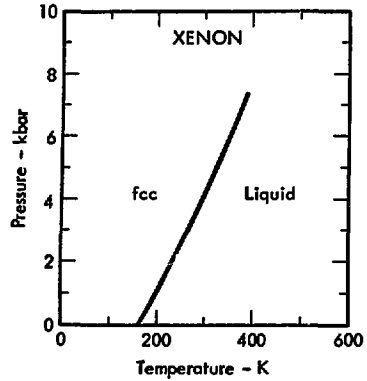

Fig. 51. The phase diagram of xenon.

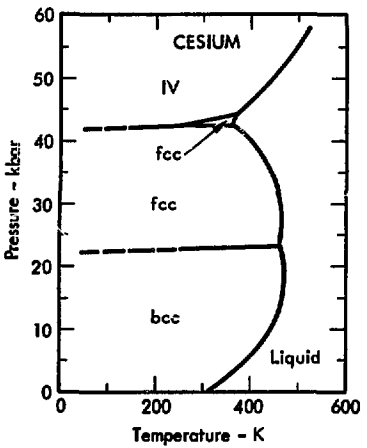

Fig. 52. The phase diagram of cesium.

room temperature the bcc phase transforms to fcc at 23 kbar.[116] Further compression yields two more phase transitions only about 1 kbar apart near 42 kbar. The first new phase is also fcc, but the structure of the second (IV) has not yet been determined.[116] The solid-solid phase boundaries have been determined,[117,118] and they show very weak temperature dependence, except that the upper fcc phase apparently disappears at low temperatures.[119]

The isostructural fcc-fcc transition occurs with a 9% volume change, and has excited much curiosity. The first theoretical attempt at an explanation proposed that the transformation represents a shift from 6s to 5d character of the conduction band.[120] Although details of this theory have been criticized, it is widely agreed to be qualitatively correct.

A further sluggish transition in solid cesium occurs near 125 kbar, accompanied by a large increase in resistance.[5a] This phase (V) exhibits superconductivity and it has been suggested that the phase is transition-metal-like, with increased d-electron character.[95]

The melting curve of cesium has been worked out to 55 kbar.[117,118] Two melting temperature maxima occur near the bcc-fcc transition. The

decreasing melting temperature of the close-packed fcc phase is due to the density of the liquid increasing beyond that of the solid. This phenomenon has been ascribed to the smearing out in the liquid of the sharp electronic transition observed in the solid. Thus the volume contraction in the liquid can be thought of as a smoothly varying change in relative concentration of two electronic species,[121] whereas in the solid this change takes place all at once. The melting curve of phase IV once again takes on a normal appearance.

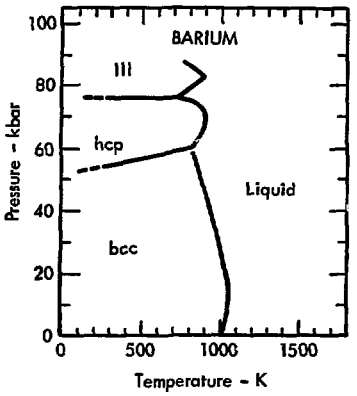

Fig. 53. The phase diagram of barium.

BARIUM

The phase diagram of barium is shown in Fig. 53. Solid barium at atmospheric pressure is bcc. At room temperature, a well-marked phase transition occurs at 55 kbar.[122] The high pressure phase has been determined to be hcp.[123] There is disagreement over the trajectory of the bcc-hcp phase boundary, since DTA measurements[124] show $dp/dT > 0$ while resistance measurements[125] show $dp/dT < 0$. Additional evidence[126] supports the first possibility, which is shown in Fig. 53. A second phase transition to a phase (III) of unknown structure has also been reported.[127,128] Stager and Drickamer[58] found a further transition at 144 kbar and room temperature, and inferred from a detailed study that this was a melting transition. Later work indicated a solid-solid transition instead.[129] A further transition at 240 kbar was found at 77K, presumably to yet another solid phase. The melting curve has been determined to about 90 kbar,[124,125,128] and three melting-curve maxima appear. It seems likely that electronic phase changes similar to those observed in cesium are occurring in barium.[130]

LANTHANUM

The phase diagram of lanthanum is shown in Fig. 54. Lanthanum exhibits three solid phases at atmospheric pressure. From 0 to 580 K, the stable phase is dhcp. At 580 K, a phase transition to an fcc phase occurs with a decrease in volume. The dhcp-fcc phase boundary has been worked out to 24 kbar.[131] At 1130 K, a transition to a bcc phase occurs, and melting occurs near 1200 K. Electrical resistance measurements[132] made to 250 kbar show a small resistance anomaly near 100 kbar, which may indicate a phase transition.

Two sets of shock wave experiments show kinks in the u_s-u_p curve for lanthanum at 250 kbar[62] and 225 kbar.[61] The first report ascribes the kink to xenon core repulsions,[62] while the second ascribes it to the intersection of the Hugoniot and the melting curve.[61] The fcc-bcc boundary and the melting curve have been determined to nearly 40 kbar.[131]

CERIUM

The phase diagram of cerium is shown in Fig. 55. This unusual diagram has been intensively studied. At zero Kelvin and atmospheric pressure, cerium is fcc. Between approximately 100 K and 450 K, a dhcp phase is stable. Between 450 K and 1000 K, the fcc phase is again stable, with the difference that the γ phase is ferromagnetic while the α phase is paramagnetic. A bcc phase then intervenes just before melting. The dhcp phase disappears at low pressures.[133]

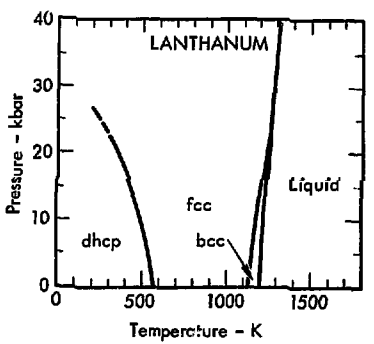

Fig. 54. The phase diagram of lanthanum.

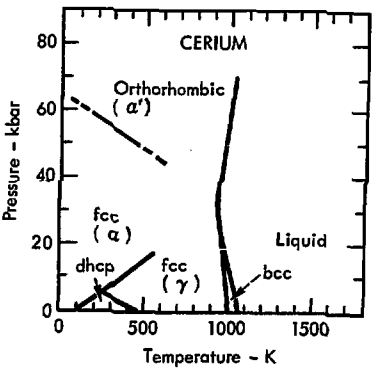

Fig. 55. The phase diagram of cerium.

The unique feature of the cerium diagram is the isostructural $\alpha \rightarrow \gamma$ phase transition, which ends in a critical point estimated from resistance measurements[134] to lie at 17.5 kbar and 550 K. A considerable theoretical effort has been made to explain the $\alpha \rightarrow \gamma$ phase transition and critical point. The earliest theories assumed that the transition represented a promotion of the localized 4f electron to the delocalized 5d band.[135] Later theories modified this by assuming only a partial 4f delocalization.[135] Such models imply a definite increase in the number of conduction elections as the pressure is increased. But this is contradicted by positron-annihilation experiments that indicate no change in the number of conduction electrons.[135] In general it could be said that the $\gamma \rightarrow \alpha$ transition results from the interaction of the 4f and conduction electrons, but the precise model of this interaction is disputed.

Further compression of cerium leads to another phase transition in the 50-60 kbar range.[136] The new phase (α') has been determined to be orthorhombic, isostructural with α-uranium.[137] The phase boundary has been determined over a relatively short temperature range, but it is interesting that extrapolation of the α-γ phase boundary and α-α' phase boundary leads to points very near one another on the melting curve. Stager and Drickamer reported a further possible phase change near 160 kbar at room temperature.[138] Two sets of shock wave data give discordant results.[61,62] In one case, a kink in the u_s-u_p curve was found at 480 kbar and ascribed to melting.[61] In the other case, no kink was found.[62]

The melting curve of cerium has been determined to 70 kbar.[134] The remarkable feature is a minimum in the melting temperature around 33 kbar. Jayaraman explains the minimum in terms of isotherms similar in shape to the supercritical isotherms observed in the vicinity of the liquid-vapor critical point.[134] These isotherms reflect the rapid decrease in the size of the cerium atoms in the solid phase as the pressure is increased.

PRASEODYMIUM

The phase diagram of praseodymium is shown in Fig. 56. Normal solid praseodymium is dhcp. A room-temperature transition to an fcc phase occurs at 40 kbar (circle).[139] The trajectory of the dhcp-fcc phase boundary is difficult to follow

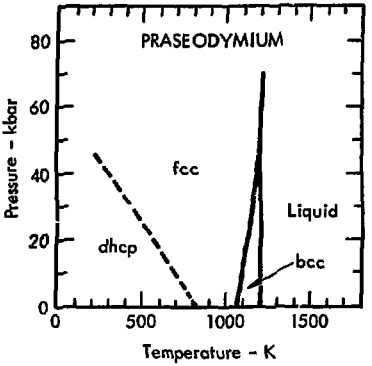

Fig. 56. The phase diagram of praseodymium.

because it is extremely sluggish and apparently quite sensitive to impurities. An approximate value for the zero-pressure transition temperature is 833 K.[140] Resistance measurements to 500 kbar show several anomalies above that at 40 kbar, and suggest two more high-pressure phases of unknown structure above the fcc phase.[138]

Two sets of shock-wave experiments show kinks in the u_s-u_p curve for praseodymium at 300 kbar[62] and 270 kbar.[61] The first report ascribes the kink to xenon-core repulsions,[62] while the second tentatively ascribes it to an electronic rearrangement in the liquid.[61] A bcc phase appears before melt. The bcc-fcc phase boundary and the melting curve have been determined to 70 kbar.[131]

NEODYMIUM

The phase diagram of neodymium is shown in Fig. 57. Under room conditions neodymium is dhcp. High pressure x-ray studies at room temperature show a transition to the fcc phase near 50 kbar (circle).[139] This transition is very difficult to detect, and the intersection of the phase boundary with the $p = 0$ axis, although suspected, could not be directly measured.[140] Instead, a temperature of 960 K is inferred from a generalized rare earth phase diagram.[141] Resistance measurements

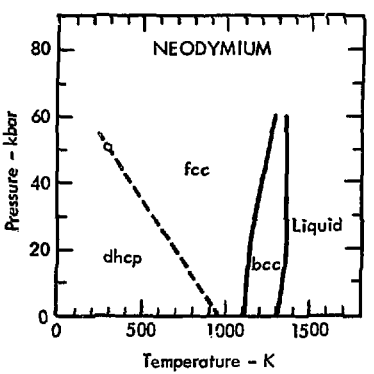

Fig. 57. The phase diagram of neodymium.

on neodymium up to 600 kbar showed anomalies in the 100-200 kbar region at different temperatures, which could correspond to another high-pressure phase transition.[138]

Two sets of shock-wave experiments show kinks in the u_s-u_p curve for neodymium at 280 kbar[62] and 250 kbar.[61] The first report ascribes the kink to xenon-core repulsions,[62] while the second identifies it with melting.[61] A bcc phase appears before melt. The bcc-fcc phase boundary and the melting curve have been determined to 60 kbar.[131]

PROMETHIUM

Promethium is dhcp at room temperature and pressure.[142] Promethium has not been extensively worked with because the element is unstable, and the most-easily available isotope has a half-life of 2.6 years. The melting temperature is 1315 K.[141] No high-pressure work has been reported.

SAMARIUM

The phase diagram of samarium is shown in Fig. 58. Under room conditions samarium has a close-packed structure of rhombohedral symmetry. The arrangement of close-packed layers in this structure is ababcbcac,

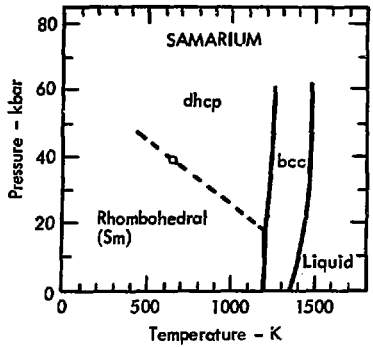

Fig. 58. The phase diagram of samarium.

henceforth called "Sm-type." Resistance measurements to 600 kbar at room temperature show anomalies near 50 kbar and 160 kbar that might correspond to phase transitions.[138] The dhcp phase appears in samarium near 40 kbar and 623 K (circle).[143]

Two sets of shock wave experiments show kinks in the u_s-u_p curve for samarium at 310 kbar[62] and 270 kbar.[61] The first report ascribes the kink to xenon-core repulsions,[62] while the second identifies it with melting.[61] A phase assumed to be bcc appears before melt. An inflection in the bcc-to-close-packed-solid phase boundary is assumed to represent the Sm-type-dhcp-bcc triple point.[131] The bcc-solid phase boundary and the melting curve have been determined to 60 kbar.[131]

EUROPIUM

The phase diagram of europium is shown in Fig. 59. Solid europium at atmospheric pressure is bcc. Below 88.6 K, europium is antiferromagnetic, with a helical arrangement of spins, and it becomes paramagnetic above this temperature. The transition has been determined to be first order,[144] which means that the bcc lattice is very slightly distorted in the magnetic phase, as in the case of chromium. The pressure dependence of the transition has been determined to 90 kbar.[145] It has been suggested that as the lattice becomes less compressible with increasing pressure, the first-order transition simply stops at about 20 kbar and gives way to a pure second-order transition.[144]

Static high-pressure resistance measurements show a sharp change near 150 kbar and room temperature, which probably corresponds to an electronic phase transition.[138] The transition pressure appears to decrease with temperature.[138] Three sets of shock wave experiments show anomalies in the u_s-u_p curve.[61,62,146] Carter et al.[61] found a discontinuity in the u_s-u_p curve at 106 kbar, and suggested that this corresponds to the intersection of Hugoniot and melting curve. Gust and Royce[62] found anomalous behavior in the 180-360 kbar range and suggested a sluggish phase transformation. Bakanova et al.[146] found a kink in the u_s-u_p curve at 386 kbar and ascribed this to an electronic rearrangement.

It is possible that the anomalies in the shock data correspond with the resistance anomaly[138] which has been ascribed to a divalent-trivalent electronic phase transition.[141] According to this theory, the anomalously divalent europium becomes more rare-earth-like as the pressure increases. The europium melting curve has been determined to 70 kbar.[147,148] A temperature maximum appears near 30 kbar. The close analogy between the behavior of europium and barium has been pointed out.[147]

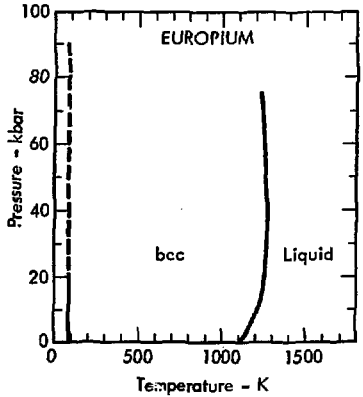

Fig. 59. The phase diagram of europium.

GADOLINIUM

The phase diagram of gadolinium is shown in Fig. 60. Under room conditions gadolinium is hcp. A transition to the samarium-type phase occurs at about 25 kbar (circle) at room temperature.[149] The hcp-Sm-type phase boundary has not been directly determined. Resistance measurements to 500 kbar show no anomalies.[60,138]

Two sets of shock wave experiments show kinks in the u_s-u_p curve for gadolinium at 260 kbar[62] and 345 kbar.[61] The first report ascribes the kink to xenon-core repulsions,[62] while the second identifies it with an electronic transition in the solid.[61] A bcc phase appears before melt, and a kink in the bcc-hcp phase boundary was taken to be hcp-Sm-type-bcc triple point.[131] The melting curve has been determined to 40 kbar.[131,148]

TERBIUM

The phase diagram of terbium is shown in Fig. 61. Under room conditions terbium is hcp. A resistance anomaly indicating a transition has been reported at 27 kbar (circle),[60] and the high pressure phase has been determined to be the Sm-type.[150] Resistance measurements to 500 kbar show smooth behavior and no clear

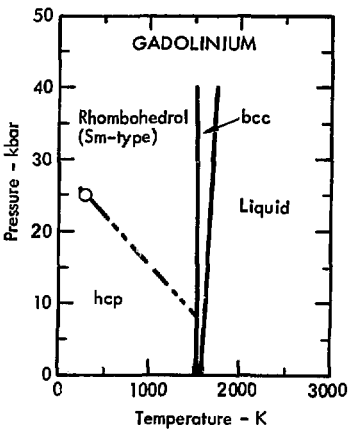

Fig. 60. The phase diagram of gadolinium.

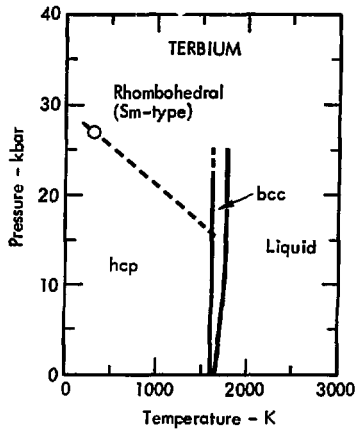

Fig. 61. The phase diagram of terbium.

evidence of further phase transitions.[138] The approximate hcp-Sm-type boundary is based on a generalized rare-earth phase diagram.[141]

Shock-wave experiments show a kink in the u_s-u_p curve at 400 kbar.[61] This is ascribed to melting.[61] The bcc-hcp phase boundary and the melting curve have been determined to about 25 kbar.[131]

DYSPROSIUM

The phase diagram of dysprosium is shown in Fig. 62. Under room conditions dysprosium is hcp. A transition to the Sm-type phase occurs at 45-50 kbar and room temperature.[60,149] Resistance measurements on dysprosium show anomalies near 200 kbar, which may indicate a phase transition.[138]

Two sets of shock-wave experiments show kinks in the u_s-u_p curve for dysprosium at 480 kbar[62] and 305 kbar.[61] The first report ascribes the kink to xenon-core repulsions,[62] while the second identifies it with melting.[61] The bcc-hcp boundary and the melting curve have been determined to 25 and 8 kbar, respectively.[131]

HOLMIUM

The phase diagram of holmium is shown in Fig. 63. Under room conditions holmium is hcp. A transition to the Sm-type phase occurs at 65 kbar[149] and room temperature. Resistance measurements on holmium to 600 kbar show no clear evidence of any further phase changes.[138]

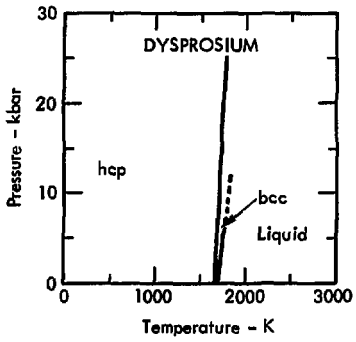

Fig. 62. The phase diagram of dysprosium.

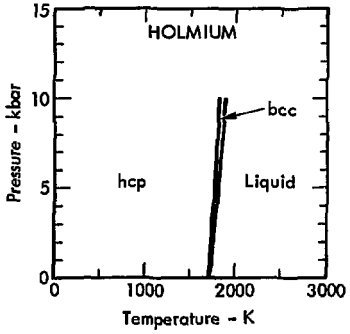

Fig. 63. The phase diagram of holmium.

Shock-wave experiments show a kink in the u_s-u_p curve of holmium at 440 kbar, which is ascribed to melting.[61] The hcp-bcc phase boundary and the melting curve have been determined to 10 kbar.[131]

ERBIUM

The phase diagram of erbium is shown in Fig. 64. Under room conditions erbium is hcp. A transition to the Sm-type phase occurs at 90 kbar.[149] Resistance measurements made to 600 kbar show no indication of a phase transition.[138]

Shock wave experiments show a kink in the u_s-u_p curve at 440 kbar, which is ascribed to melting.[61] No bcc phase has been detected before melt.[131] The melting curve has been determined to 10 kbar.[131]

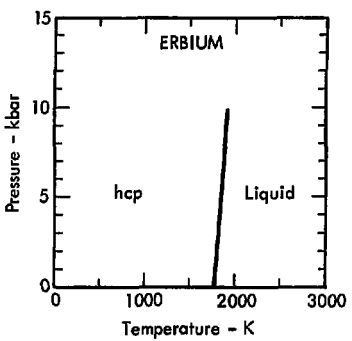

Fig. 64. The phase diagram of erbium.

THULIUM

The phase diagram of thulium is shown in Fig. 65. Under room conditions thulium is hcp. A transition to the Sm-type phase occurs at room temperature near 110 kbar.[149] Resistance measurements to 500 kbar show no clear evidence of any further phase changes.[138]

Shock-wave experiments show a kink in the u_s-u_p curve, which is ascribed to melting.[61] No bcc phase has been detected before melt.[131] The melting curve has been determined to 10 kbar.[131]

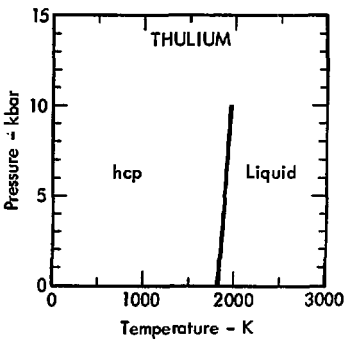

Fig. 65. The phase diagram of thulium.

YTTERBIUM

The phase diagram of ytterbium is shown in Fig. 66. Below 300 K

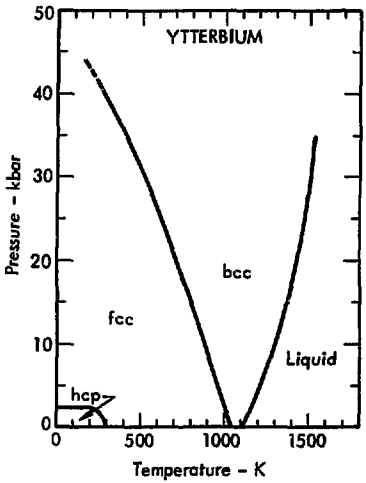

Fig. 66. The phase diagram of ytterbium.

and 2 kbar, ytterbium exists in a diamagnetic hcp phase.[151] A martensitic phase transformation at 300 K and atmospheric pressure produces a paramagnetic fcc phase. The hcp-fcc phase boundary has been determined, and it is clear that the hcp phase disappears above 2 kbar.[152]

At room temperature, increasing pressure causes a series of changes in resistivity. Below 20 kbar ytterbium behaves like a metal, between 20 and 40 kbar it behaves like a semiconductor, and at 40 kbar a phase change takes place to a bcc metallic phase.[153] These changes have been explained in terms of the opening and closing of band gaps with increasing pressure.[154] The fcc-bcc phase boundary has been determined,[147] and it intersects the p = 0 axis above 1000 K.

Stephens[148] reports that a new hcp phase appears between the fcc and bcc phases below 15 kbar, but this may be the result of impurities. A pressure-independent resistance anomaly variously observed at 743 K[147] and 898 K,[155] has been ascribed to another phase transition. Static compression of ytterbium at room temperature to 280 kbar shows no further resistance anomalies above 40 kbar.[153]

Three sets of shock-wave experiments show kinks in the u_s-u_p curve at 130 kbar,[62] 160 kbar,[61] and 490 kbar.[146] The kinks are ascribed to xenon-core repulsion, melting, and electronic phase transitions, respectively. Johansson and Rosengren consider the 130 kbar anomaly to indicate an electronic phase transition involving a shift from the divalent to the trivalent ionic state in the solid.[141] The melting curve has been determined to 35 kbar.[147] The ytterbium phase diagram closely resembles that of strontium.

LUTETIUM

The phase diagram of lutetium is shown in Fig. 67. Solid lutetium at low pressures is hcp. Compression to 230 kbar at room temperature causes a transition to the Sm-type lattice.[156] The hcp-Sm-type phase boundary has not been determined. The melting curve has been determined to 10 kbar.[131]

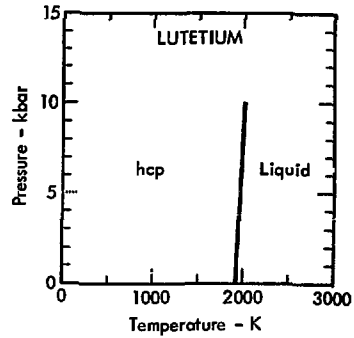

Fig. 67. The phase diagram of lutetium.

HAFNIUM

Under room conditions hafnium is hcp. At atmospheric pressure a transition occurs near 2270 K to a bcc phase. The bcc phase is slightly more dense than the hcp, implying a negative value of dp/dT for the phase boundary. A static-high-pressure *search for the hexagonal ω phase* found in titanium and zirconium failed to show any change of phase.[157]

Three sets of shock-wave experiments showed anomalies in the u_s-u_p curve.[62,66,146] Gust and Royce[62] ascribed a kink at 600 kbar to xenon-core repulsion. McQueen, *et al.*[66] ascribed a discontinuity at 400 kbar to a solid-solid phase transition. Bakanova, *et al.*[146] ascribed a kink at 450 kbar to an electronic transition. Hafnium melts at 2495 K.[63] The melting curve has not been reported.

TANTALUM

The phase diagram of tantalum is shown in Fig. 68. Solid tantalum is bcc. An approximate melting curve has been determined to 60 kbar.[158]

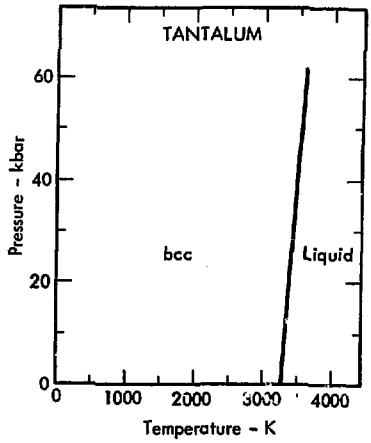

Fig. 68. The phase diagram of tantalum.

TUNGSTEN

The phase diagram of tungsten is shown in Fig. 69. Solid tungsten is bcc. An approximate melting curve has been determined to 50 kbar.[159]

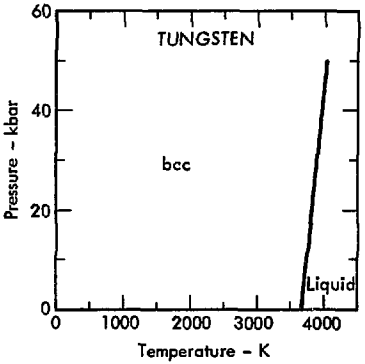

Fig. 69. The phase diagram of tungsten.

RHENIUM

Solid rhenium is hcp. Static compression of rhenium at room temperature to 350 kbar showed no phase transitions.[160] Rhenium melts at 3433 K.[63] The melting curve has not been reported.

OSMIUM

Solid osmium is hcp. Osmium melts at 3300 K.[63] The melting curve has not been determined.

IRIDIUM

Solid iridium is fcc. Room temperature compression to 175 kbar showed no phase transition.[161] Iridium melts at 2716 K.[63] The melting curve has not been reported.

PLATINUM

The phase diagram of platinum is shown in Fig. 70. Solid platinum is fcc. The melting curve has been approximately determined to 50 kbar.[159,162]

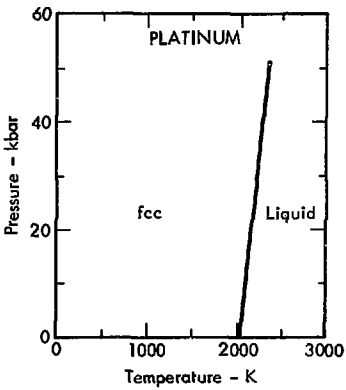

Fig. 70. The phase diagram of platinum.

GOLD

The phase diagram of gold is shown in Fig. 71. Solid gold is

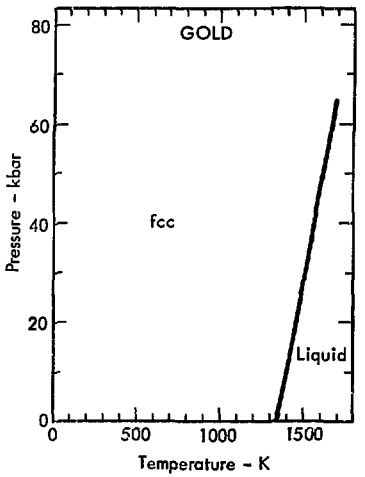

Fig. 71. The phase diagram of gold.

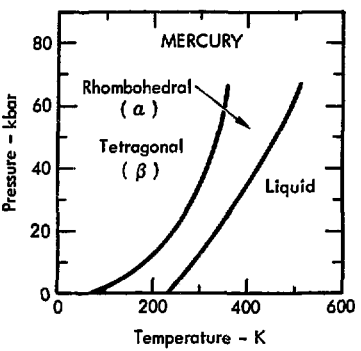

Fig. 72. The phase diagram of mercury.

fcc. The melting curve has been determined to 65 kbar.[75]

MERCURY

The phase diagram of mercury is shown in Fig. 72. Solid mercury at low temperatures has a body centered tetragonal structure. In this phase each atom has two nearest neighbors and eight second nearest neighbors. With increasing temperature, a transformation to a rhombohedral structure occurs. This structure may be regarded as a distorted fcc lattice. The tetragonal-rhombohedral phase boundary has been determined to 65 kbar.[163]

A third phase, named γ, has been found at very low temperatures by straining the solid. Its structure and equilibrium phase boundaries have not yet been determined.[164] The melting curve of mercury has been determined to 65 kbar.[163]

THALLIUM

The phase diagram of thallium is shown in Fig. 73. Below 500 K at atmospheric pressure, thallium is hcp. Above 500 K, it is bcc. A high pressure fcc phase occurs above 35 kbar and 388 K. The solid-solid phase boundaries have been determined to 60 kbar.[78] The melting curve has been determined to 50 kbar.[78]

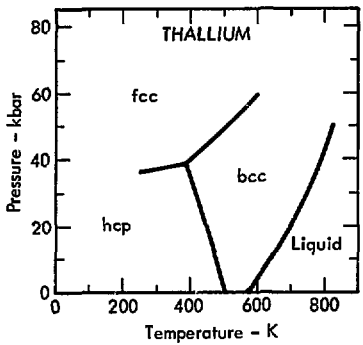

Fig. 73. The phase diagram of thallium.

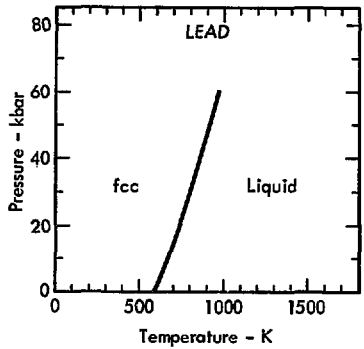

Fig. 74. The phase diagram of lead.

LEAD

The phase diagram of lead is shown in Fig. 74. Solid lead at low pressure is fcc. At 137 kbar and room temperature a transition to a hcp phase occurs.[165,166] The phase boundary has not been determined. The melting curve has been determined to 60 kbar.[77]

BISMUTH

The phase diagram of bismuth is shown in Fig. 75. This diagram is of special importance to high pressure physics because its many phase transitions have been used as calibration standards. There is still controversy over the existence of some transitions, and rather little x-ray structure work has been done on the high pressure phases. The low pressure solid phase is rhombohedral, isostructural with arsenic and antimony. Conflicting claims have been made for the structure of phase II, with no clear agreement.[1] Duggin[83] suggests that phase III is tetragonal, similar to the high pressure phase of arsenic. A study of phase VI at 90 kbar at room temperature has shown it to be bcc.[167] The phase boundaries shown are a synthesis of several studies.[84,168,169] The phases IX, VIII, and VI meet in a triple point at 135 kbar,[169] and the VI-IX phase boundary then proceeds to higher pressures. This boundary was presumably detected in a study at room temperature and 300 kbar.[170] The melting curve has been determined to 55 kbar.[84]

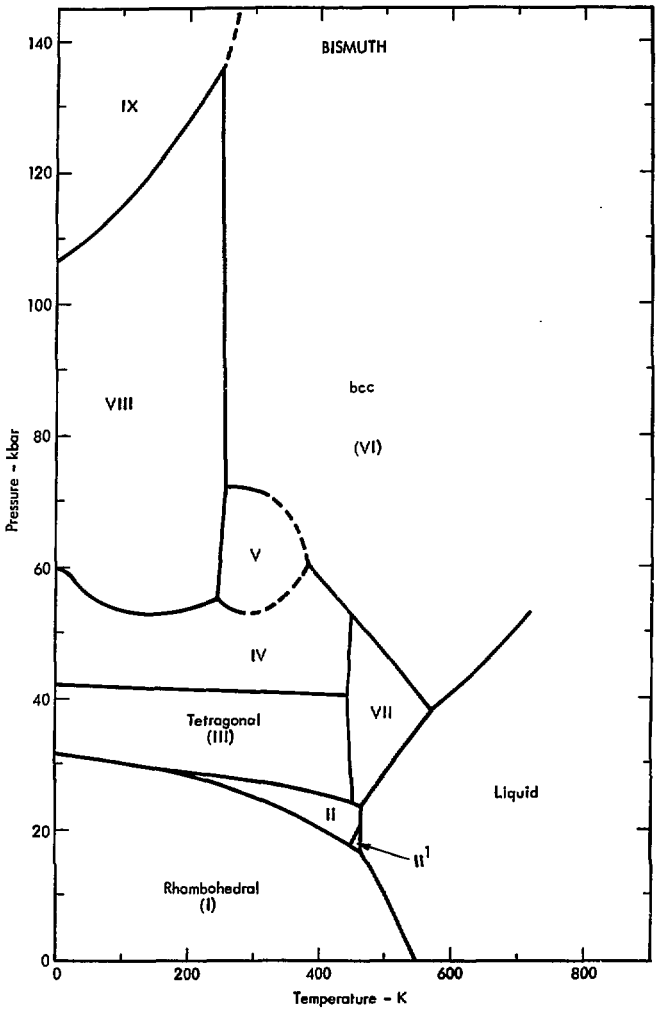

Fig. 75. The phase diagram of bismuth.

POLONIUM

At atmospheric pressure and below room temperature, polonium has a simple cubic structure, the only known example of this structure in the elements at zero pressure. A sluggish phase transition occurs somewhere near room temperature (291-327 K)[171] to a simple rhombohedral form which is a slight distortion of the simple cubic. The rhombohedral form is slightly more dense,[171] leading to a negative dp/dT. The phase boundary has not been determined. Polonium melts at 519 K.[63] The melting curve has not been reported.

ASTATINE

Astatine is a very unstable element and its physical properties have not been determined.

RADON

The crystal structure of solid radon has not been reported. Radon melts at 202 K.[172] The melting curve has not been determined.

FRANCIUM

Francium is a very unstable element and its physical properties have not been determined.

RADIUM

Solid radium is bcc at room temperature. Radium melts at 973 K.[63] No high pressure work has been reported.

ACTINIUM

Solid actinium is fcc at room temperature. Actinium melts at 1323 K.[63] No high pressure work has been reported.

THORIUM

Solid thorium under room conditions is fcc. Superconductivity measurements to 160 kbar show an anomaly that could be due to a phase change near 70 kbar.[173] At atmospheric pressure near 1670 K, thorium transforms to a bcc phase. The volume change of the transition is zero to within experimental error.[1] The trajectory of the phase boundary has not been reported. Thorium melts at 2024 K.[63] The melting curve has not been determined.

PROTACTINIUM

Solid protactinium under room conditions is body centered tetragonal. Metal solidified from the melt is fcc, suggesting that this is the high

temperature form of the solid.[1] No direct measurements of phase transitions have been made, however. Protactinium melts at about 1810 K.[174] No high pressure work has been reported.

URANIUM

The phase diagram of uranium is shown in Fig. 76. Under room conditions solid uranium has an orthorhombic structure with four atoms per unit

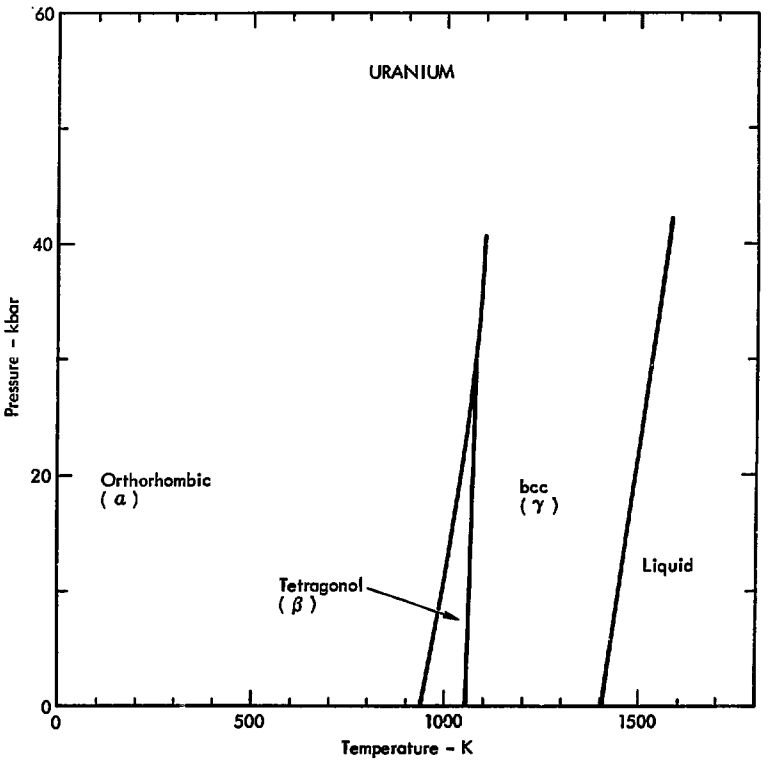

Fig. 76. The phase diagram of uranium.

cell. At 940 K and atmospheric pressure, a transition to a complex tetragonal form with 30 atoms per unit cell occurs. The precise space group remains to be determined.[1] At 1050 K another phase transition leads to a bcc phase. The solid-solid phase boundaries have been determined, and indicate a triple point for the three phases near 30 kbar.[175] The melting curve has been determined to 40 kbar.[176]

NEPTUNIUM

The phase diagram of neptunium is shown in Fig. 77. Under room conditions neptunium is orthorhombic, with eight atoms per unit cell and two distinct types of atomic positions. At 550 K and atmospheric pressure a phase transition to a tetragonal phase with four atoms per unit cell and two types of atomic positions occurs. A bcc phase appears above 840 K. The solid-solid phase boundaries and the melting curve have been determined to 35 kbar.[177]

PLUTONIUM

The phase diagram of plutonium is shown in Figs. 78 and 79. The plutonium diagram is very complex. All but one of the seven known solid phases exist at atmospheric pressure. The low pressure portion of the phase diagram and its high pressure continuation are shown in separate figures. The low temperature α phase is monoclinic, with 16 atoms per unit cell and 8 crystallographically distinct types of atomic positions. The β phase is also monoclinic, with 34 atoms per unit cell and 7 types of positions. Both of these structures are quite irregular and are difficult to correlate with close-packed forms.

At high pressure only α and β exist, and the α-β phase boundary shows a temperature maximum. The β phase transforms to orthorhombic γ below 3.5 kbar and to ζ, with undetermined structure, above this pressure. There is a β-ζ-liquid triple point near 27 kbar.

The next two phases are fcc (δ) and body centered tetragonal (δ'), which exist only at low pressures. The δ' phase is followed by bcc (ε), which melts to a more dense liquid. The tetragonal δ' phase is intermediate in structure between fcc and bcc. The ε phase disappears at a triple point below 20 kbar. The solid-solid phase boundaries and the melting curve have been determined to 140 kbar.[174,178-180]

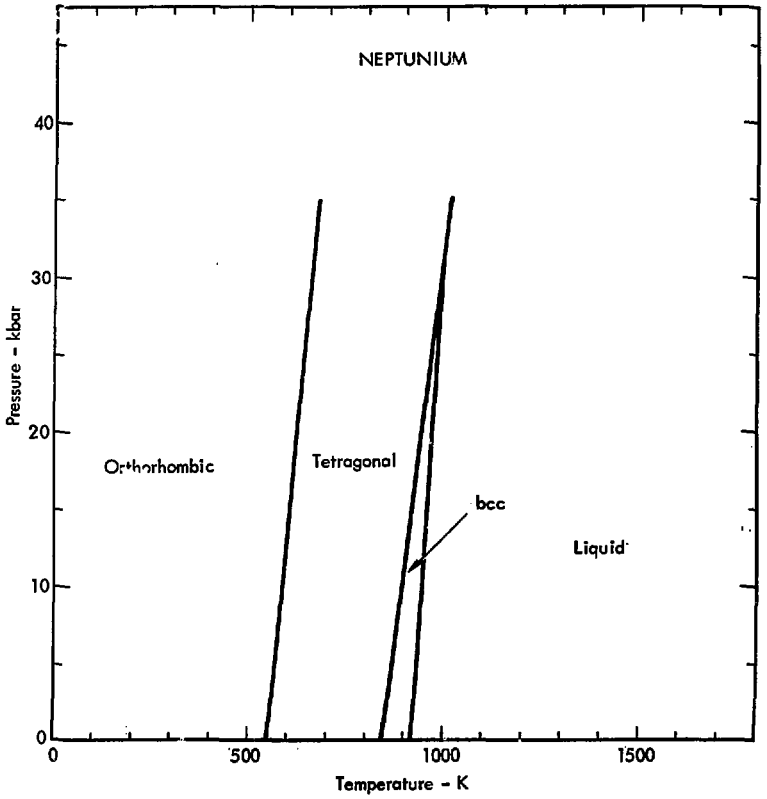

Fig. 77. The phase diagram of neptunium.

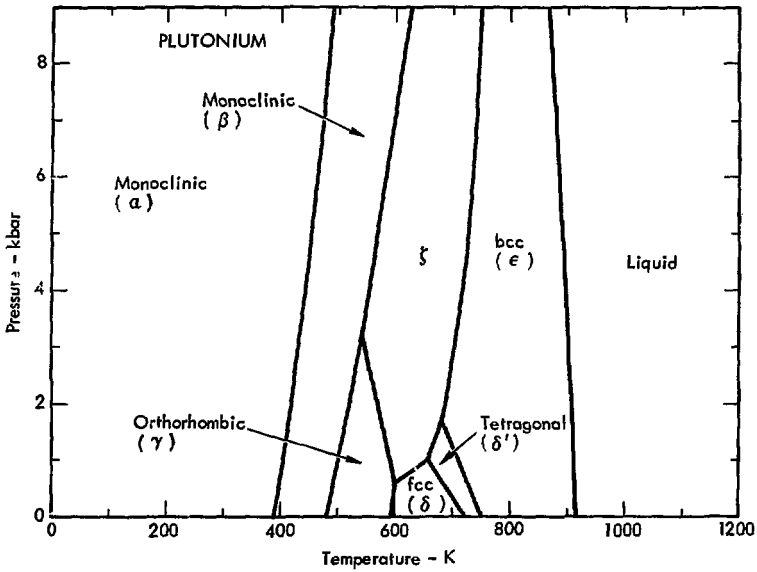

Fig. 78. The phase diagram of plutonium.

AMERICIUM

The phase diagram of americium is shown in Fig. 80. Americium under room conditions is dhcp. There is evidence for a transition to an fcc phase at 920 ± 50 K,[181] but with very little change in volume. The dhcp-fcc phase boundary is therefore approximately represented by a vertical dashed line in Fig. 80. Static compression of americium at room temperature shows a resistance change at 90 kbar, which may represent a continuation of the dhcp-fcc phase boundary.[182] Heating at atmospheric pressure above 1300 K leads to a new phase, which Stephens et al. suggest is bcc.[182] The fcc-bcc phase boundary and melting curves have been determined to 35 kbar.[182]

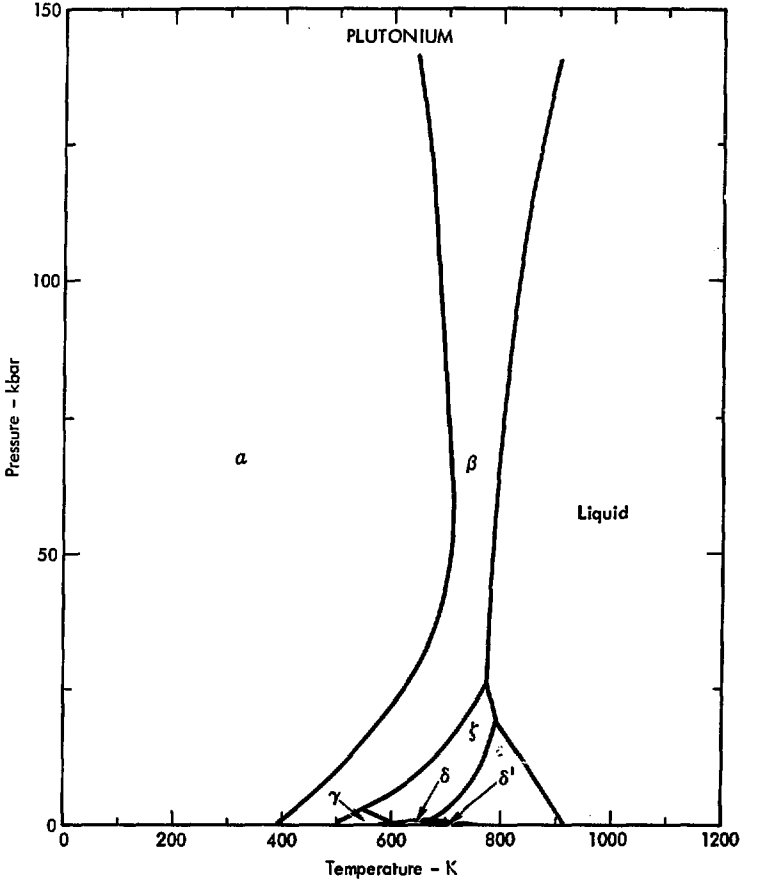

Fig. 79. The phase diagram of plutonium.

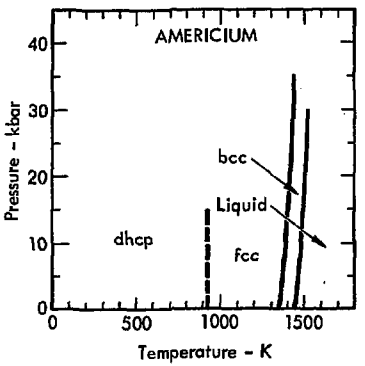

Fig. 80. The phase diagram of americium.

CURIUM

Depending on the method of preparation, curium metal is found to have either an fcc or a dhcp structure under room conditions.[1] The fcc phase has the higher density.[1] No phase boundary has been reported. The estimated melting point is 1620 K.[174] No high pressure work has been reported.

BERKELIUM

Berkelium metal prepared by high temperature reduction contains a mixture of dhcp and fcc structures.[1] Here the dhcp phase is the more dense.[1] The estimated melting point is 1260 K.[174] No high pressure work has been reported.

References

1. J. Donohue, The Structures of the Elements (Wiley, New York, 1974).

2. W. Klement, Jr., and A. Jayaraman, Progr. Solid State Chem. 3, 289 (1966).

3. V. V. Evdokimova, Soviet Phys. Usp. English Transl. 9, 54 (1966) [Usp. Fiz. Nauk 88, 93 (1966)].

4. J. F. Cannon, J. Phys. Chem. Ref. Data 3, 781 (1974).

5. L. Meyer, Adv. Chem. Phys. 16, 343 (1969).

6. R. J. Lee and J. C. Raich, Phys. Rev. B5, 1591 (1972).

7. S. A. Dickson and H. Meyer, Phys. Rev. 138, A 1293 (1965).

8. J. Felsteiner and Z. Friedman, Phys. Rev. B8, 3996 (1973).

9. G. A. Neece, F. J. Rogers, and W. G. Hoover, J. Comp. Phys. 7, 621 (1971).

10. R. L. Mills and E. R. Grilly, Phys. Rev. 101, 1246 (1956).

11. J. Wilks, Liquid and Solid Helium (Clarendon Press, Oxford, 1967).

12. W. E. Keller, Helium - 3 and Helium - 4 (Plenum Press, New York, 1969).

13. O. V. Lounasmaa, Contemp. Phys. 15, 353 (1974).

14. D. Gugan, Can. J. Phys. 41, 1381 (1963).

15. R. Stager and H. G. Drickamer, Phys. Rev. 132, 124 (1963).

16. H. D. Luedemann and G. C. Kennedy, J. Geophys. Res. 73, 2795 (1968).

17. M. Francois and M. Contre, Conference International sur la Metallurgie du Beryllium (Grenoble, 1965) p. 201.

18. A. R. Marder, Science 142, 664 (1963).

19. H. D. Stromberg and D. R. Stephens, An Automatic Calibration System for Measuring Electrical Resistance at High Pressures, ASME, Rept. 64 - WA/PT - 13 (1965).

20. L. F. Vereshchagin, A. A. Semerchan, S. V. Popova, and N. N. Kuzin, Soviet Phys. Doklady English Trsnsl. 7, 692 (1963) [Dokl. Akad. Nauk SSSR 145, 757 (1962)].

21. R. H. Wentorf, Science 147, 49 (1965).

22. N. D. Stout, Lawrence Livermore Laboratory personal communication (July, 1975).

23. N. D. Stout, R. W. Mar, and W. O. J. Boo, High Temp. Sci. 5, 241 (1973).

24. F. P. Bundy, H. P. Bovenkerk, H. M. Strong, and R. H. Wentorf, Jr., J. Chem. Phys. 35, 383 (1961).

25. R. G. McQueen and S. P. Marsh, LASL Rept. GMX - 6 - 607 (unpublished, no date) p. 41.

26. B. J. Alder and R. H. Christian, Phys. Rev. Lett. 7, 367 (1961).

27. L. F. Vereshchagin, E. N. Yakovlev, B. V. Vinogradov, V. P. Sakun, and G. N. Stepanov, High Temp. - High Press. 6, 505 (1974).

28. N. S. Fateeva and L. F. Vereshchagin, JETP Lett. English Transl. 13, 110 (1971) [ZhETF Pis. Red. 13, 157 (1971)].

29. A. F. Schuch and R. L. Mills, J. Chem. Phys. 52, 6000 (1970).

30. C. A. Swenson, J. Chem. Phys. 23, 1963 (1955).

31. J. D. Grace and G. C. Kennedy, J. Phys. Chem. Solids 28, 977 (1967).

32. R. Stevenson, J. Chem. Phys. 27, 673 (1957).

33. R. L. Mills and E. R. Grilly, Phys. Rev. 99, 480 (1955).

34. J. A. Jahnke, J. Chem. Phys. 47, 336 (1967).

35. G. C. Straty and R. Prydz, Phys. Lett. 31A, 301 (1970).

36. R. K. Crawford and W. B. Daniels, J. Chem. Phys. 55, 5651 (1971).

37. H. G. Drickamer, R. W. Lynch, R. L. Clendenen, and E. A. Perez-Albuerne, Solid State Phys. 19, 135 (1966).

38. G. C. Kennedy and R. C. Newton, in Solids Under Pressure, W. Paul and D. W. Warschauer, Eds. (McGraw-Hill Book Co, New York, 1963) Ch. 7.

39. N. N. Roy and E. G. Steward, Nature 224, 905 (1969).

40. J. Lees and B. H. J. Williamson, Nature 208, 278 (1965).

41. S. Minomura and H. G. Drickamer, J. Phys. Chem. Solids 23, 451 (1962).

42. J. C. Jamieson, Science 139, 762 (1963).

43. R. H. Wentorf, Jr., and J. S. Kasper, Science 139, 338 (1963).

44. F. P. Bundy, J. Chem. Phys. 41, 3809 (1964).

45. W. H. Gust and E. B. Royce, J. Appl. Phys. 42, 1897 (1971).

46. J. C. Jamieson, Science 139, 1291 (1963).

47. R. E. Harris, R. J. Vaisnys, H. Stromberg, and G. Jura, in Progress in Very High Pressure Research, F. P. Bundy, W. R. Hubbard, Jr., and H. M. Strong, Eds. (Wiley, New York, 1961) p. 165.

48. L. J. Long, G. B. Guarise, and A. Marani, Corsi Semin. Chim. 5, 97 (1967).

49. A. Marani, G. B. Guarise, Chim. Ind. (Milan) 50, 663 (1968).

50. G. C. Vezzoli, F. Dachille, and R. Roy, Science 168, 218 (1969).

51. G. C. Vezzoli, F. Dachille, and R. Roy, Inorg. Chem. 8, 2658 (1969).

52. G. C. Vezzoli, F. Dachille, and R. Roy, J. Polymer Sci., Part A-1, 7, 1557 (1969).

53. G. C. Vezzoli and R. J. Zeto, Inorg. Chem. 9, 2478 (1970).

54. R. E. Harris and G. Jura in Elemental Sulfur, B. Meyer, Ed. (Interscience, New York, 1965) p. 179.

55. S. Block and G. J. Piermarini, High Temp.-High Press. 5, 567 (1973).

56. S. E. Babb, Jr., J. Chem. Phys. 50, 5271 (1969).

57. A. Jayaraman, W. Klement, Jr., and G. C. Kennedy, Phys. Rev. 132, 1620 (1963).

58. R. A. Stager and H. G. Drickamer, Phys. Rev. 131, 2524 (1963).

59. L. F. Vereshchagin, A. A. Semerchan, N. N. Kuzin, and Yu. A. Sadkov, Soviet Phys. Doklady English Transl. 14, 557 (1969) [Dokl. Akad. Nauk SSSR 186, 1045 (1969)].

60. H. D. Stromberg and D. R. Stephens, J. Phys. Chem. Solids 25, 1015 (1964).

61. W. J. Carter, J. N. Fritz, S. P. Marsh, and R. G. McQueen, J. Phys. Chem. Solids 36, 741 (1975).

62. W. H. Gust and E. B. Royce, Phys. Rev. B8, 3595 (1973).

63. K. A. Gschneidner, Jr., Solid State Phys 16, 275 (1964).

64. F. P. Bundy, Phase Diagram of Titanium, General Electric, Rept. 63-RL-3481C (1963).

65. A. Jayaraman, W. Klement, Jr., and G. C. Kennedy, Phys. Rev. 131, 644 (1963).

66. R. G. McQueen, S. P. Marsh, J. W. Taylor, J. N. Fritz, and W. J. Carter, in High-Velocity Impact Phenomena, R. Kinslow, Ed. (Academic Press, New York, 1970) Ch. 7.

67. M. O. Steinitz, L. H. Schwartz, J. A. Marcus, E. Fawcett, and W. A. Reed, Phys Rev. Lett. 23, 979 (1969).

68. H. Umebayashi, G. Shirane, B. C. Frazer, and W. B. Daniels, J. Phys. Soc. Japan 24, 368 (1968).

69. T. Mitsui and C. T. Tomizuka, Phys. Rev. 137, A 564 (1965).

70. W. E. Evenson and H. T. Hall, Science 150, 1164 (1965).

71. E. Rapoport and G. C. Kennedy, J. Phys. Chem. Solids. 27, 93 (1966).

72. F. P. Bundy, J. Appl. Phys. 36, 616 (1965).

73. H. M. Strong, R. E. Tuft, and R. E. Hanneman, Metall. Trans. 4, 2657 (1973).

74. H. M. Strong and F. P. Bundy, Phys. Rev. 115, 278 (1959).

75. J. Akella and G. C. Kennedy, J. Geophys. Res. 76, 4969 (1971).

76. R. W. Lynch and H. G. Drickamer, J. Phys. Chem. Solids 26, 63 (1965).

77. J. Akella, J. Ganguly, R. Grover, and G. Kennedy, J. Phys. Chem. Solids 34, 631 (1973).

78. A. Jayaraman, W. Klement, Jr., R. C. Newton, and G. C. Kennedy, J. Phys. Chem. Solids 24, 7 (1963).

79. W. Buckel and W. Gey, Z. Phys'k 176, 336 (1963).

80. W. H. Gust and E. B. Royce, J. Appl. Phys. 43, 4437 (1972).

81. C. H. Bates, F. Dachille, and R. Roy, Science 147, 860 (1965).

82. L. F. Vereshchagin, A. A. Semerchan, N. N. Kuzin, and S. V. Popova, Soviet Phys. Doklady English Transl. 6, 41 (1961) [Dokl. Akad. Nauk SSSR 136, 320 (1961)].

83. M. J. Duggin, J. Phys. Chem. Solids 33, 1267 (1972).

84. W. Klement, Jr., A. Jayaraman, and G. C. Kennedy, Phys. Rev. 131, 632 (1963).

85. A. S. Balchan and H. G. Drickamer, J. Chem. Phys. 37, 1948 (1961).

86. B. M. Riggleman and H. G. Drickamer, J. Chem. Phys. 37, 446 (1962).

87. D. R. McCann and L. Cartz, J. Chem. Phys. 56, 2552 (1972).

88. W. Klement, Jr., L. H. Cohen, and G. C. Kennedy, J. Phys. Chem. Solids 27, 171 (1966).

89. I. E. Paukov, E. Yu. Tonkov, and D. S. Mirinskii, Russ. J. Phys. Chem. English Transl. 41, 995 (1967) [Zh. Fiz. Khim. 41, 1857 (1967).

90. C. Susse, R. Epain, and B. Vodar, Compt. Rend. 258, 4513 (1964).

91. C. E. Weir, G. J. Piermarini, and S. Block, J. Chem. Phys. 50, 2089 (1969).

92. P. H. Lahr and W. G. Eversole, J. Chem. Eng. Data 7, 42 (1962).

93. F. P. Bundy and H. M. Strong, Solid State Phys. 13, 81 (1962).

94. D. B. McWhan, T. M. Rice, and P. H. Schmidt, Phys. Rev. 177, 1063 (1969).

95. J. Wittig, Phys. Rev. Lett. 24, 812 (1970).

96. N. B. Brandt, I. V. Berman, and Yu. P. Kurkin, JETP Lett. English Transl. 20, 8 (1974) [Zh ETF Fis. Red. 20, 20 (1974)].

97. L. F. Vereshchagin, A. A. Semerchan, N. N. Kuzin, and S. V. Popova, Soviet Phys. Doklady English Transl. 6, 391 (1961) [Dokl. Akad. Nauk SSSR 138, 84 (1961)].

98. N. S. Fateeva and L. F. Vereshchagin, JETP Lett. English Transl. 14, 153 (1974) [ZhETF Pis. Red. 14, 233 (1971)].

99. R. L. Clendenen and H. G. Drickamer, J. Phys. Chem. Solids 25, 865 (1964).

100. L. Liu and W. A. Bassett, J. Appl. Phys. 44, 1475 (1973).

101. R. W. Vaughan and H. G. Drickamer, J. Phys. Chem. Solids 26, 1549 (1965).

102. I. N. Nikolaev, N. P. Mar'in, V. N. Panyushkin, and L. S. Pavlykov, Soviet Phys. Solid State English Transl. 14, 2022 (1973).[Fiz. Tverd. Tela 14, 2337 (1972)].

103. A. Jayaraman, W. Klement, Jr., and G. C. Kennedy, Phys. Rev. 130, 540 (1963).

104. T. D. Barnett, V. E. Bean, and H. T. Hall, J. Appl. Phys. 37, 875 (1965).

105. T. N. Kolobyanina, S. S. Kabalkina, L. F. Vereshchagin, and L. V. Fedina, Soviet Phys. JETP English Transl. 28, 88 (1969) [Zh. Eksp. Teor. Fiz. 55, 164 (1968)].

106. S. S. Kabalkina, T. N. Kolobyanina, and L. F. Vereshchagin, Soviet Phys. JETP English Transl. 31, 259 (1970) [Zh. Eksp. Teor. Fiz. 58, 486 (1970)].

107. S. M. Stishov and N. A. Tikhomirova, Soviet Phys. JETP English Transl. 21, 810 (1965) [Zh. Eksp. Teor. Fiz. 48, 1215 (1965)].

108. J. C. Jamieson and D. B. McWhan, J. Chem. Phys. 43, 1149 (1965).

109. I. V. Berman, Zh. I. Bynzarov, and Yu. P. Kurkin, Soviet Phys. Solid State English Transl. 14, 2192 (1973) [Fiz. Tverd. Tela 14, 2527 (1972)].

110. F. A. Blum, Jr., and B. C. Deaton, Phys. Rev. 137, A 1410 (1965).

111. R. Grover, A. S. Kusubov, and H. D. Stromberg, J. Chem. Phys. 47, 4398 (1967)

112. S. S. Kabalkina, T. N. Kolobyanina, and L. F. Vereshchagin, Soviet Phys. Doklady English Transl. 12, 50 (1967) [Dokl. Akad. Nauk SSSR 172, 313 (1967)].

113. B. M. Riggleman and H. G. Drickamer, J. Chem. Phys. 38, 2721 (1963).

114. B. J. Alder and R. H. Christian, Phys. Rev. Lett. 4, 450 (1960).

115. W. Klement, Jr., L. H. Cohen, and G. C. Kennedy, J. Chem. Phys. 44, 3697 (1966).

116. H. T. Hall, L. Merrill, and J. D. Barnett, Science 146, 1297 (1964).

117. G. C. Kennedy, A. Jayaraman, and R. C. Newton, Phys. Rev. 126, 1363 (1962).

118. A. Jayaraman, R. C. Newton and J. M. McDonough, Phys. Rev. 159, 527 (1967).

119. D. B. McWhan and A. L. Stevens, Solid State Commun. 7, 301 (1969).

120. R. Sternheimer, Phys. Rev. 78, 235 (1950).

121. E. Rapoport, Phys. Rev. Lett. 19, 345 (1967).

122. J. C. Haygarth, I. C. Getting, and G. C. Kennedy, J. Appl. Phys. 38, 4557 (1967).

123. J. D. Barnett, R. B. Bennion, and H. T. Hall, Science 141, 534 (1963).

124. A. Jayaraman, W. Klement, Jr., and G. C. Kennedy, Phys. Rev. Lett. 10, 387 (1963).

125. B. C. Deaton and D. E. Bowen, Appl. Phys. Lett. 4, 97 (1964).

126. C. Susse and R. Epain, J. Chim. Phys. 63, 1580 (1966).

127. J. P. Bastide, C. Susse, and R. Epain, Compt. Rend. Ser. C 267, 857 (1968).

128. J. P. Bastide and C. Susse, High Temp.-High Press. 2, 237 (1970).

129. H. G. Drickamer, Solid State Phys. 17, 1 (1965).

130. J. Wittig and B. Matthias, Phys. Rev. Lett. 22, 634 (1969).

131. A. Jayaraman, Phys. Rev. A 139, 690 (1965).

132. L. F. Vereshchagin, A. A. Semerchan, and S. V. Popova, Soviet Phys. Doklady English Transl. 6, 488 (1961) [Dokl. Akad. Nauk SSSR 138, 1059 (1961)].

133. K. A. Gschneidner, Jr., R. O. Elliot, and R. R. MacDonald, J. Phys. Chem. Solids 23, 555 (1962).

134. A. Jayaraman, Phys. Rev. 137, A 179 (1965).

135. R. F. Gempel, D. R. Gustafson, and J. D. Willenberg, Phys. Rev. B5, 2082 (1972).

136. E. King, J. A. Lee, I. R. Harris, and T. F. Smith, Phys. Rev. B1, 1380 (1970).

137. F. H. Ellinger and W. H. Zacharisen, Phys. Rev. Lett. 32, 773 (1974).

138. R. A. Stager and H. G. Drickamer, Phys. Rev. 133, A 830 (1964).

139. G. J. Piermarini and C. E. Weir, Science 144, 69 (1964).

140. E. Bucher, C. W. Chu, J. P. Maita, K. Andres, A. S. Cooper, E. Buehler, and K. Nassau, Phys. Rev. Lett. 22, 1260 (1969).

141. B. Johansson and A. Rosengren, Phys. Rev. B11, 2836 (1975).

142. P. G. Pallmer and T. D. Chikalla, J. Less-Common Metals 24, 233 (1971).

143. A. Jayaraman and R. C. Sherwood, Phys. Rev. 134, A 691 (1964).

144. R. L. Cohen, S. Hufner, and K. W. West, Phys. Rev. 184, 263 (1969).

145. D. B. McWhan, P. C. Souers, and G. Jura, Phys. Rev. 143, 385 (1966).

146. A. A. Bakanova, I. P. Dudoladov, and Yu. N. Sutulov, Soviet Phys. Solid State English Transl. 11, 1515 (1970) [Fiz. Tverd. Tela 11, 1881 (1969)].

147. A. Jayaraman, Phys. Rev. 135, A 1056 (1964).

148. D. R. Stephens, J. Phys. Chem. Solids 26, 943 (1965).

149. D. B. McWhan and A. L. Stevens, Phys. Rev. 154, 438 (1967).

150. D. R. Stephens and Q. Johnson, J. Less-Common Metals 17, 243 (1969).

151. E. Bucher, P. H. Schmidt, A. Jayaraman, K. Andres, J. P. Maita, K. Nassau, and P. D. Dernier, Phys. Rev. B2, 3911 (1970).

152. M. Rieux and D. Jerome, Solid State Comm. 9, 1179 (1971).

153. R. A. Stager and H. G. Drickamer, Science 139, 1284 (1963).

154. P. C. Souers and G. Jura, Science 140, 481 (1963).

155. H. T. Hall and L. Merrill, Inorg. Chem. 2, 618 (1963).

156. L. Liu, J. Phys. Chem. Solids 36, 31 (1975).

157. J. C. Jamieson, Science 140, 72 (1963).

158. N. S. Fateeva and L. F. Vereshchagin, Soviet Phys. Doklady English Transl. 16, 322 (1970) [Dokl. Akad. Nauk SSSR 197, 1060 (1971)].

159. L. F. Vereshchagin and N. S. Fateeva, Soviet Phys. JETP English Transl. 28, 597 (1969) [Zh. Eksp. Teor. Fiz. 55, 1145 (1968)].

160. L. Liu, T. Takahashi, and W. A. Bassett, J. Phys. Chem. Solids 31, 1345 (1970).

161. R. N. Schock and Q. Johnson, Phys. Met. Metallog. English Transl. 31, No. 5, 213 (1971) [Fiz. Metal. Metalloved 31, 1101 (1971)].

162. N. R. Mitra, D. L. Decker, and H. B. Vanfleet, Phys. Rev. 161, 613 (1967).

163. W. Klement, Jr., A. Jayaraman, and G. C. Kennedy, Phys. Rev. 131, 1 (1963).

164. J. S. Abell, A. G. Crocker, and H. W. King, Phil. Mag. 21, 207 (1970).

165. T. Takahasi, H. K. Mao, and W. A. Bassett, Science 165, 1352 (1969).

166. H. Mii, I. Fujishiro, M. Senoo, and K. Ogawa, High Temp.-High Press. 5, 155 (1973).

167. P. Schaufelberger, H. Merx, and M. Contre, High Temp.-High Press. 5, 221 (1973).

168. N. A. Tikhomirova, E. Yu. Tonkov, and S. M. Stishov, JETP Lett. English Transl. 3, 60 (1966) [ZhFET Pis. Red. 3, 96 (1966)].

169. C. G. Homan, J. Phys. Chem. Solids (to be published).

170. C. G. Homan, T. E. Davidson, and D. P. Kendall, Appl. Phys. Lett. 26, 615 (1975).

171. J. M. Goode, J. Chem. Phys. 26, 1269 (1957).

172. G. L. Pollock, Rev. Mod. Phys. 36, 748 (1964).

173. W. A. Fertig, A. R. Moodenbaugh, and M. B. Maple, Phys. Lett. 38A, 517 (1972).

174. J. A. Lee and M. B. Waldron, Contemp. Phys. 13, 113 (1972).

175. W. Klement, Jr., A. Jayaraman, and G. C. Kennedy, Phys. Rev. 129, 1971 (1973).

176. J. Ganguly and G. C. Kennedy, J. Phys. Chem. Solids 34, 2272 (1973).

177. D. R. Stephens, J. Phys. Chem. Solids 27, 1201 (1966).

178. D. R. Stephens, J. Phys. Chem. Solids 24, 1197 (1963).

179. R. G. Liptai and R. J. Friddle, J. Less-Common Metals 10, 297 (1966).

180. C. Roux, P. le Roux, and M. Rapin, J. Nucl. Mater. 40, 305 (1971).

181. D. B. McWhan, B. B. Cunningham, and J. C. Wallman, J. Inorg. Nucl. Chem. 24, 1025 (1962).

182. D. R. Stephens, H. D. Stromberg, and E. M. Lilley, J. Phys. Chem. Solids 29, 815 (1968).

RBC/gw

Appendix A: The Space Lattices

Lattice	Axes	Angles
primitive (simple) cubic body-centered cubic face-centered cubic	$a = b = c$	$\alpha = \beta = \gamma = 90°$
primitive tetragonal body-centered tetragonal	$a = b \neq c$	$\alpha = \beta = \gamma = 90°$
primitive orthorhombic base-centered orthorhombic body-centered orthorhombic face-centered orthorhombic	$a \neq b \neq c$	$\alpha = \beta = \gamma = 90°$
primitive monoclinic base-centered monoclinic	$a \neq b \neq c$	$\alpha = \gamma = 90° \neq \beta$
triclinic	$a \neq b \neq c$	$\alpha \neq \beta \neq \gamma$
rhombohedral	$a = b = c$	$\alpha = \beta = \gamma$
hexagonal	$a = b \neq c$	$\alpha = \beta = 90°, \gamma = 120°$